The Spatiotemporal Variability, Trends, and Drivers of Winter Arctic Polynyas

CARMEN HAU MAN WONG,[a] CÉLINE HEUZÉ,[a] LUISA ICKES,[b] AND LU ZHOU[c]

[a] *Department of Earth Sciences, University of Gothenburg, Gothenburg, Sweden*
[b] *Department of Space, Earth, and Environment, Chalmers University of Technology, Gothenburg, Sweden*
[c] *Institute for Marine and Atmospheric Research Utrecht, Utrecht University, Utrecht, Netherlands*

(Manuscript received 5 June 2025, in final form 4 November 2025, accepted 5 January 2026)

ABSTRACT: Polynyas, thin-ice or open water regions within the sea ice, have regularly been observed in the Arctic since satellite observations began in the 1970s. Their opening, in response to complex interactions between several drivers, significantly influences the regional weather and climate, ecosystem, and ocean circulation. Yet their monitoring at the pan-Arctic scale is rare since their detection is not trivial. Here, we use three sea ice satellite data products to detect and investigate major Arctic polynya events since 1978, focusing on their winter locations and total area. We compute the polynyas' recurrence percentage, total number, and area, varying the sea ice concentration (30%–60%) and thickness (10–30 cm) thresholds to enhance our analysis robustness. We find that the most active polynya regions are along the coasts of the Laptev Sea, Kara Sea, Franz Josef Land, northwestern Greenland, and Chukchi Sea. Both total and cumulative polynya areas have significant increasing trends in these regions and at the pan-Arctic scale between 1978 and 2024. In these regions, we find that wind speed and direction have a prominent 1-day lag effect on polynya openings, suggesting that they are latent heat polynyas. The air temperature plays a preconditioning role in many regions but seems to impact most the daily area extent, after the polynyas formed. Under rising temperatures and stronger extreme winds, our results suggest an increase in Arctic polynya activity, although polynyas might then extend into the open ocean, where different processes would drive their opening.

KEYWORDS: Arctic; Sea ice; Atmosphere-ocean interaction; Climate change; Climate variability; Satellite observations

1. Introduction

Polynyas, open water regions within the sea ice cover, are crucial sites for ice and deep-water formation as well as air–sea surface energy exchanges in polar regions. Since satellite passive microwave observations became available in polar regions four decades ago, this natural phenomenon has been observed regularly in the open ocean and coastal areas (Gordon and Comiso 1988; Preußer et al. 2016). Polynyas were classified into two major types in early studies: coastal (latent heat) polynyas and open water (sensible heat) polynyas. Coastal polynyas form where there are divergent ice motions driven by dynamical drivers (e.g., wind, ocean currents), usually along the coast (Smith et al. 1990; Morales Maqueda et al. 2004). Meanwhile, open water polynyas form away from the coast due to abnormal thermodynamic drivers (e.g., oceanic heat intrusion), causing sea ice to melt at the ocean surface (Smith et al. 1990; Morales Maqueda et al. 2004). In addition, it is possible that mechanical and thermal forcings have similar contributions to the polynya formation, and this type is, therefore, called hybrid latent and sensible polynyas (Bailey et al. 2004; Hirano et al. 2016).

Most Arctic polynyas are coastal polynyas, known for their high ice production on site (Tamura and Ohshima 2011). Polynyas expose the relatively warm water surface to cold air, and the strong heat loss from the ocean to the atmosphere causes subsequent ice refreeze (Morales Maqueda et al. 2004). This sea ice production enhances the upper-ocean salinity via brine rejection; polynyas are, therefore, crucial for deep-water formation (Aagaard et al. 1981; Martin and Cavalieri 1989). The vigorous air–sea interaction also modifies the surface heat and moisture budgets, intensifying the local turbulent mixing, influencing regional atmospheric dynamics, and promoting Arctic cloud formation (Gultepe et al. 2003; Boisvert et al. 2012; Monroe et al. 2021). Biogeochemistry processes are also affected by polynya openings, with more gaseous exchange in winter and primary productivity in early spring at the open water surface (Else et al. 2013; Marchese et al. 2017; Moore et al. 2023). Determining and understanding the causes of the precise polynya locations is essential, as this is the required first step to quantify their contributions to the local and regional climate in the Arctic. However, these locations and formation frequency may change: The Arctic is warming significantly, nearly 4 times faster than the rest of the world (Rantanen et al. 2022). The wind strength is also likely to increase, according to model projections, as sea ice retreat reduces surface roughness (Mioduszewski et al. 2018). In an increasingly uncertain Arctic climate, it is crucial to establish with more certainty the relationship between winter Arctic polynyas and their drivers.

Early Arctic polynya research relied mainly on passive microwave satellite-retrieved sea ice concentration (SIC), as they are ground-truth data with good spatial and temporal coverage (Martin and Cavalieri 1989; Cavalieri and Martin 1994; Bareiss and Görgen 2005). The data are on a daily scale, regardless of nighttime or dense cloud cover, which permits their observation even in polar winter (Tamura and Ohshima

Denotes content that is immediately available upon publication as open access.

Corresponding author: Carmen Hau Man Wong, hau.man.wong@gu.se

DOI: 10.1175/JCLI-D-25-0312.1

TABLE 1. Summary of the passive-microwave-based satellite product datasets used in this study.

Satellite data product	Spaceborne sensor	Temporal coverage (resolution)	Spatial resolution (km)	Data range
SIC	SMMR, SSM/I, and SSMIS	1978–2024 (daily)	25	0%–100%
	AMSR-E and AMSR2	2002–11 (daily, AMSR-E)	6.25	
		2012–24 (daily, AMSR2)		
SIT	SMOS and SMOS–SMAP	2010–24 (daily)	12.5	0–50 cm

2011). With the improvement of satellite measurements, recent polynya research has put more emphasis on thin sea ice thickness (SIT) retrieval as ice production and salt flux at polynya sites can be quantified at the same time (Tamura and Ohshima 2011; Iwamoto et al. 2014; Preußer et al. 2016). These studies, however, often focus on the regional scale along the Arctic coast, predominantly along the Laptev coast, Canadian coast, and Chukchi coast, where polynyas recur almost every year and concurrent in situ data (e.g., moorings) are available (Ingram et al. 2002; Willmes et al. 2011; Hirano et al. 2016). Long-term, pan-Arctic polynya research is still rare. The last pan-Arctic polynya mapping was conducted around a decade ago by Preußer et al. (2016), covering the period 2002–18, with the objective of quantifying ice production rather than investigating polynya dynamics. Here, we not only conduct an updated pan-Arctic polynya mapping but also quantify trends and variability in this crucial natural phenomenon using satellite-retrieved winter sea ice concentration and thickness during the period 1978–2024. Furthermore, to explain the trends that we observe in the different regions of the Arctic Ocean, we determine the relationship between polynya openings and total area and their atmospheric drivers.

Section 2 describes the sea ice satellite products and atmospheric data used in this study. Section 3 describes our novel Arctic polynya detection method and the methodology for the calculated results and climate variables. Section 4 presents the spatial and temporal polynya trends from a pan-Arctic to a regional perspective, as well as the analysis of their atmospheric drivers. We then briefly summarize our results and add concluding remarks in section 5.

2. Satellite products and atmospheric reanalysis data

a. SIC

We use two daily SIC datasets from the National Snow and Ice Data Center (NSIDC) and the University of Bremen Sea Ice Remote Sensing group (Table 1). Data are accessible online at the NSIDC (https://nsidc.org/data/nsidc-0051/versions/2) and the University of Bremen Sea Ice Remote Sensing website (https://seaice.uni-bremen.de/start/). NSIDC SIC data are derived from the brightness temperature T_b data received by the *Nimbus-7* Scanning Multichannel Microwave Radiometer (SMMR) and the Defense Meteorological Satellite Program (DMSP) Special Sensor Microwave Imager (SSM/I)–Special Sensor Microwave Imager/Sounder (SSMIS). The multichannel satellites of these observation programs measure the frequency from 6 to 91 GHz horizontally and vertically (NSIDC 2024). The raw data are then processed by the NASA Team algorithm, using the horizontal and vertical polarizations of the 18/19-GHz channel, as well as the vertical gradient ratio between frequencies of 18/19 GHz and 37 GHz (Cavalieri et al. 1984; Comiso et al. 1997; Cavalieri et al. 1999). The SIC product has a daily temporal coverage from 1978 to 2024 with a 25-km spatial resolution.

The other SIC dataset that we use is obtained from the University of Bremen Sea Ice Remote Sensing group. It is also derived from T_b data captured by the Advanced Microwave Scanning Radiometer for EOS (AMSR-E) and the Advanced Microwave Scanning Radiometer 2 (AMSR2) (Spreen et al. 2008). It has an observation period from 2002 to 2024, during which there is a 9-month data gap between 2011 and 2012 (Spreen et al. 2008). AMSR-E and AMSR2 take measurements in six frequency bands from 6.9 to 89 GHz. SIC is derived from the Arctic Radiation and Turbulence Interaction Study (ARTIST) Sea Ice algorithm using 89-GHz data, which has a higher spatial resolution than the NASA Team algorithm (Spreen et al. 2008). The SIC retrieval algorithm also resolves the influences of clouds and water vapor by introducing weather filters which are calculated from data at 18-, 23-, and 37-GHz channels (Spreen et al. 2008). The retrieved SIC is provided on 6.25 km × 6.25 km grid cells (Table 1).

b. SIT

The SIT product that we use, which is provided by the University of Bremen Sea Ice Remote Sensing group, is derived from the spaceborne passive microwave sensors Soil Moisture Ocean Salinity (SMOS) and Soil Moisture Active Passive (SMAP) brightness temperature data at 1.4 GHz (L band; Huntemann et al. 2014; Tian-Kunze et al. 2014; Paţilea et al. 2019, see Table 1). SMOS measurements started in 2010, providing more than 10 years of T_b data for SIT retrieval thus far. The SMOS SIT is retrieved from an empirical algorithm by Huntemann et al. (2014), utilizing the L band at incident angles of 40° and 50°. After SMAP was launched in 2015, a novel SIT retrieval algorithm combining T_b data from SMOS and SMAP was derived by Paţilea et al. (2019). The SMOS–SMAP algorithm complements the original SMOS algorithm by Huntemann et al. (2014) as SMOS–SMAP T_b data have a 6% increase of spatial coverage (Paţilea et al. 2019). This combined daily SIT dataset covers the period 2010–24 with a 12.5-km spatial resolution. In general, SIT is retrieved up to 50 cm; most research agrees that 50 cm is the maximum ceiling to have reliable SIT results and a reasonable uncertainty range (Kaleschke et al. 2012; Huntemann et al. 2014; Paţilea et al. 2019).

c. Atmospheric drivers

We use the fifth generation European Centre for Medium-Range Weather Forecasts atmospheric reanalysis (ERA5)

hourly data for our trend and climatology analyses of the potential polynya drivers (Hersbach et al. 2020). ERA5 data have a spatial resolution of 0.25° × 0.25°, which is approximately equivalent to 25 km × 25 km in the Arctic. Given that the satellite products used in this study have a daily temporal resolution, we use the hourly data at 0000, 0600, 1200, and 1800 in UTC time stamps, averaging them to produce a daily mean value. The precise values of hourly atmospheric data are not critical to our overall trend analysis, and the diurnal cycle of the Arctic Ocean in the polar winter is negligible. Most Arctic polynyas have been identified as coastal or hybrid polynyas in previous studies (e.g., Tamura and Ohshima 2011; Ren et al. 2022), which means that wind is an essential factor driving polynyas to open. Meanwhile, Pease (1987) found that the near-surface air temperature has a strong impact in determining the size of a polynya. Therefore, we use the 2-m air temperature (T2m), 10-m u component of wind (U10), 10-m v component of the wind (V10), and the wind speed (WS) computed from U10 and V10 to identify potential drivers of polynya activity. Additionally, we also use the downward surface thermal radiation (DLR), surface sensible heat flux (SSHF), and surface latent heat flux (SLHF) to investigate the interplay of atmospheric temperature and wind on polynya opening, before and after the opening.

3. Arctic polynya retrieval

a. Data analysis period

The data analysis period is based on the availability of the three satellite datasets we just described: 1978–2024 (SMMR, SSM/I & SSMIS), 2002–24 (AMSR-E & AMSR2), and 2012–24 (SMOS & SMOS–SMAP). We only analyze polynyas formed in wintertime for each year. In this study, we define the winter period from December to March as the sea ice cover is most stable in this time period and to reduce seasonal sea ice uncertainty close to the ice edge.

Due to an observation gap between AMSR-E & AMSR2, the 2011/12 winter is skipped for the AMSR-E & AMSR2 SIC results. As we explain in the next section, our SIT-based polynya retrieval requires concurrent AMSR-E & AMSR2 data, so we do not show SMOS & SMOS–SMAP results for the 2011/12 winter either. Additionally, we did not process SMOS & SMOS–SMAP data in the 2010/11 winter because of the large areas with missing data within the study region.

b. Polynya detection each winter

The polynya detection algorithm is summarized in Fig. 1. We separate the sea ice regions from open oceans and land with a flood-fill algorithm. Flood-fill algorithms change adjacent values to a common value if they are similar, starting from a "seed" point. Due to the geometry of the Arctic, the flood filling has to be initiated with several seeds in the open Atlantic and Pacific Oceans (Fig. 1a, orange stars). The algorithm masks grid cells below a certain sea ice threshold as being part of the open ocean, filtering out the sea ice cover. The study area is then limited to latitudes 65°–90°N, and only open water regions within the sea ice cover are analyzed (Fig. 1b). In the next step, we apply a SIC or SIT threshold to the analysis region: Grid cells with values below the threshold will be defined as open water (potential polynyas) and those above as sea ice (Fig. 1c). Threshold values are determined by a sensitivity test, as we describe in the next subsection. Finally, we want to ensure that the potential polynyas are within the sea ice cover, where the maximum extent is usually defined as SIC ≥ 15%. For the SIC products, the SIC threshold range is always above 15%. For the SIT products, we need an extra step and keep only the SIT grid cells where SIC is above 15%, i.e., within the sea ice extent. To do so, we downgraded the spatial resolution of the AMSR-E/AMSR2 SIC data from 6.25 to 12.5 km to match the SIT product's horizontal resolution. If any potential polynya as detected by SIT is outside the sea ice extent from the downgraded AMSR-E/AMSR2, it is removed from the results (Fig. 1d).

We create a base map to indicate all the polynya locations for each day. We use the label() function from the Python SciPy package (Virtanen et al. 2020) to count the cumulative number of polynyas on the base map. This function considers grid cells that are adjacently connected and diagonally connected as part of the same polynya. From the daily base maps, we generate winter base maps and calculate the recurrence percentage at each grid cell. A high recurrence percentage means high polynya activity. We use the recurrence percentage maps to investigate the polynya spatial distribution across the Arctic for the last 46 winters. For pan-Arctic and regional analyses, we also compute polynya area time series. The cumulative winter polynya area is the sum of all open water grid cells across the study region on the daily base map for one winter; the total winter polynya area is the sum of all grid cells that have been identified at least once as a polynya in one winter.

c. Sea ice threshold sensitivity test

SIT and SIC are each sensitive to different ice processes, and their products have different resolutions and observation periods. Therefore, it is essential to determine a SIC–SIT threshold pair to make our results consistent over their common time period (i.e., after 2010). We conduct a sensitivity test on the downscaled AMSR-E & AMSR2 SIC (12.5 km), used to determine whether SIT-retrieved polynyas are inside the sea ice extent each day (see section 3b), and the SMOS & SMOS–SMAP SIT dataset. Theoretically, the cumulative polynya area for each winter extracted by SIC and SIT should be the same. SIC and SIT will not have the same values in practice due to different satellite sensors, frequency bands, and retrieval algorithms. Therefore, we calculate the area differences of SIC and SIT to decide which threshold pairs have the least deviation in area. We compute the winter cumulative polynya area over the common time period (2012–24) using the different thresholds mentioned in the literature (Table 2): We vary the SIC thresholds from 30% to 60% with an interval of 10% and the SIT thresholds from 10 to 30 cm with an interval of 5 cm. The SIC–SIT threshold pair with the smallest area deviation can produce consistent results. The average yearly area differences are then normalized relative to 0,

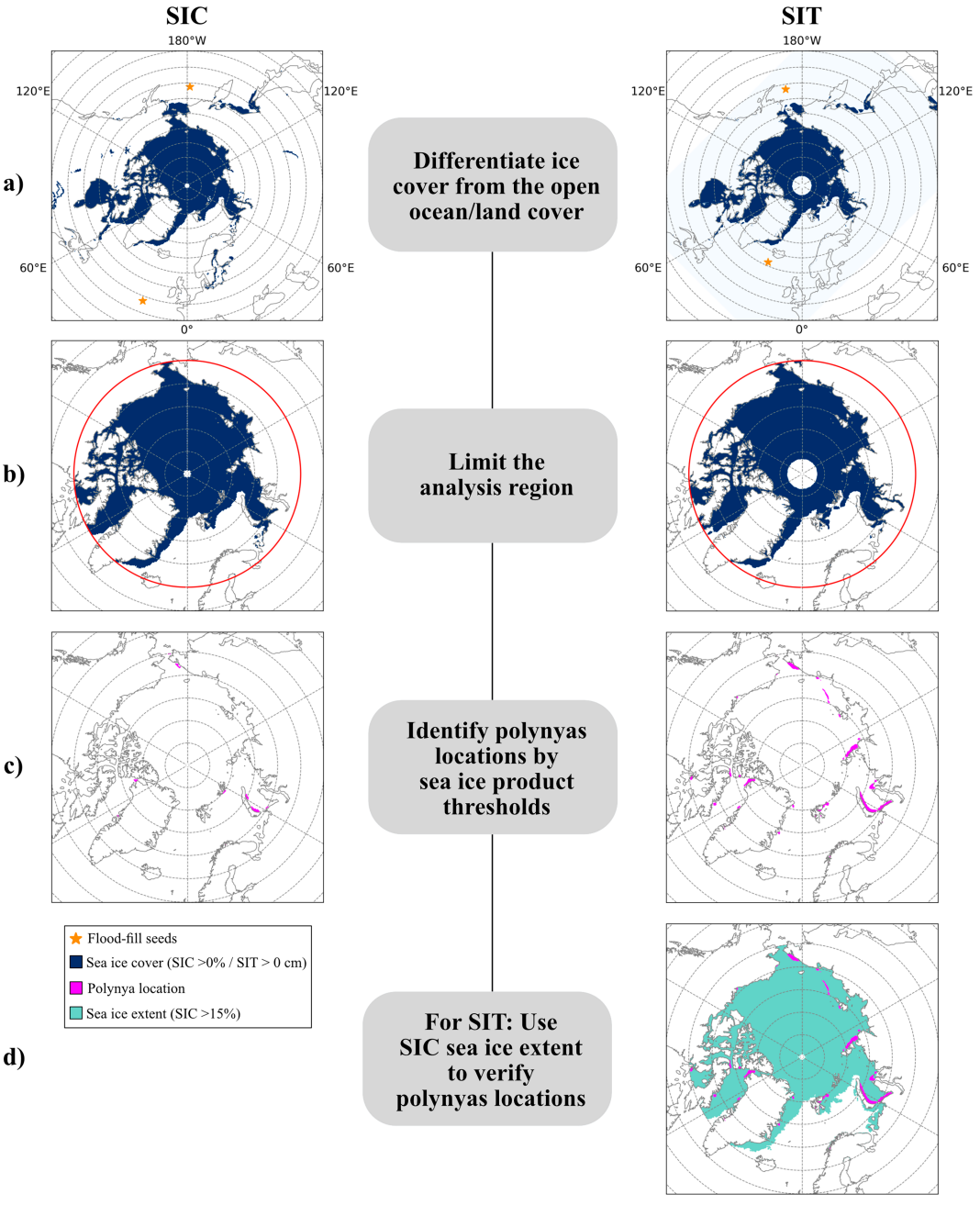

FIG. 1. Flowchart of the polynya detection process: (a) use a flood-fill algorithm to separate sea ice and open ocean and land, (b) limit the analysis region to 65°–90°N, (c) identify potential polynya locations using our detection algorithm with specific sea ice product thresholds, and (d) an extra step for SIT: use SIC 15% sea ice extent to verify polynya locations.

which is the most ideal case without area differences between SIC and SIT. The normalized results are presented in Fig. 2. As expected, some pairs have differences close to or of 1, i.e., are impossible, for example, thick sea ice but low concentration. Similarly, thin ice with a high concentration returns an error of nearly 0.5. The pair with the smallest cumulative area difference is 30% SIC and 10-cm SIT, as well as 50% SIC and 20-cm SIT (error of 0.04). Most previous studies used the higher threshold values for sea ice products as they identify more, connected grid cells as open water, resulting in a more robust polynya count (Campbell et al. 2019). Therefore, SIC 50% would be a better choice than SIC 30%. Additionally, the 50% SIC and 20-cm SIT threshold pair is also the most prevalent threshold option in earlier studies (Table 2). Therefore, 50% SIC and 20-cm SIT is the one we choose for the rest of our analysis.

TABLE 2. Summary of SIC/SIT thresholds applied in previous Arctic or Antarctic polynya studies.

Sea ice products	Threshold	Reference
SIT	10 cm	Martin et al. (2004)
	12 cm	Nakata et al. (2015), Mohrmann et al. (2021)
	15 cm	Tamura and Ohshima (2011)
	20 cm	Martin et al. (2004), Adams et al. (2013), Preußer et al. (2015, 2016), Ren et al. (2022)
	25 cm	—
	30 cm	Smedsrud et al. (2006)
SIC	30%	Kawaguchi et al. (2011), Tamura and Ohshima (2011), Mohrmann et al. (2021)
	40%	Campbell et al. (2019)
	50%	Dokken et al. (2002), Campbell et al. (2019), Shen et al. (2021), Bennett et al. (2024)
	≥60%	Massom et al. (1998), Campbell et al. (2019), Monroe et al. (2021), Zhou et al. (2022), Landrum et al. (2024)

d. Trends and driver analysis in the polynya regions

We examine the evolution of all winter Arctic polynyas and, for each region, the correlation with atmospheric variables potentially driving this evolution across the study period. To do so, we determine the specific regions of interest by computing the polynya recurrence percentage of the spatial distribution map for each satellite dataset, for the observation period of that dataset. Then, a general area is identified both visually as having a high percentage of recurrence (purple regions) and also based on regions frequently studied in previous research (listed in Table 2). We quantify the trend in polynya opening frequency (i.e., opening recurrence for each winter), total polynya area, and cumulative polynya area by linear least squares regression over the entire dataset period for the pan-Arctic and regional values.

To explain the trend results, we perform a lagged correlation analysis between the daily on–off opening state and the daily polynya area with atmospheric variables, using the Pearson correlation. The on–off state of a polynya grid cell indicates whether, on that day, the polynya is open (value of 1) or closed (0). We also compute the trends for four atmospheric drivers: T2m, WS, U10, and V10 (see section 2c), using the same method as for the polynyas. The time for a winter polynya to form and become stable typically takes between half a day and 4 days, which implies that there is a time lag for atmospheric forcings to impact the development of a polynya (Pease 1987). Thus, we perform a lagged correlation analysis, with a slightly longer time lag of up to 7 days. We test both instantaneous and lagged correlations to investigate the lag effect of atmosphere and fluxes on polynyas and of polynya openings on atmosphere and fluxes. For each grid cell, we calculate the correlation coefficient for all lag days and select the day with the highest absolute coefficient value to represent the time with the most significant lag effect. After that, we obtain the total number of grid cells for each lag day. All results presented are statistically significant at or above the 90% level, verified by the Student's *t* test.

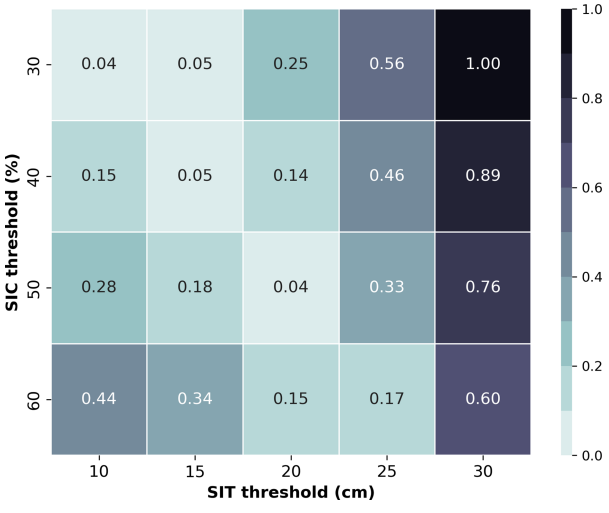

FIG. 2. Sea ice product threshold sensitivity results. Normalized values represent the average yearly area differences between SIC and SIT retrieval results.

4. Results and discussion

a. Spatial distribution of Arctic winter polynyas

The Arctic polynya recurrence for all years is consistent among all three satellite products, showing that most polynyas are formed along coastlines (Fig. 3). For most of the regions considered (all except regions five—East Siberian Sea, seven—Beaufort Sea, and nine—North East Water), the satellite products result in 50% or more recurrence (Fig. 3a). Spatial patterns are consistent, but the recurrence magnitude differs between products due to their different spatial resolutions and time periods. Note that most of these purple regions along the coast have previously been identified as major Arctic polynyas, in terms of high ice production rate, by previous studies that applied different retrieval methods based on radiation emission (Tamura and Ohshima 2011; Iwamoto et al. 2014; Preußer et al. 2016). More locations are identified as polynyas by our algorithm when the spatial resolution of the sea ice product increases: 40.7% of the grid cells have a nonzero polynya frequency in the 6.25-km resolution AMSR-E & AMSR2; 35.8% in the 12.5-km SMOS & SMOS–SMAP; and 19.6% in the 25-km SMMR, SSM/I & SSMIS. AMSR-E & AMSR2 (Fig. 3d) and SMOS & SMOS–SMAP results (Fig. 3e) both reveal a band of strong polynya activity from east of Greenland to north of Svalbard, a location close to the ice edge. Our algorithm differentiates polynyas from the sea ice edge using a SIC threshold

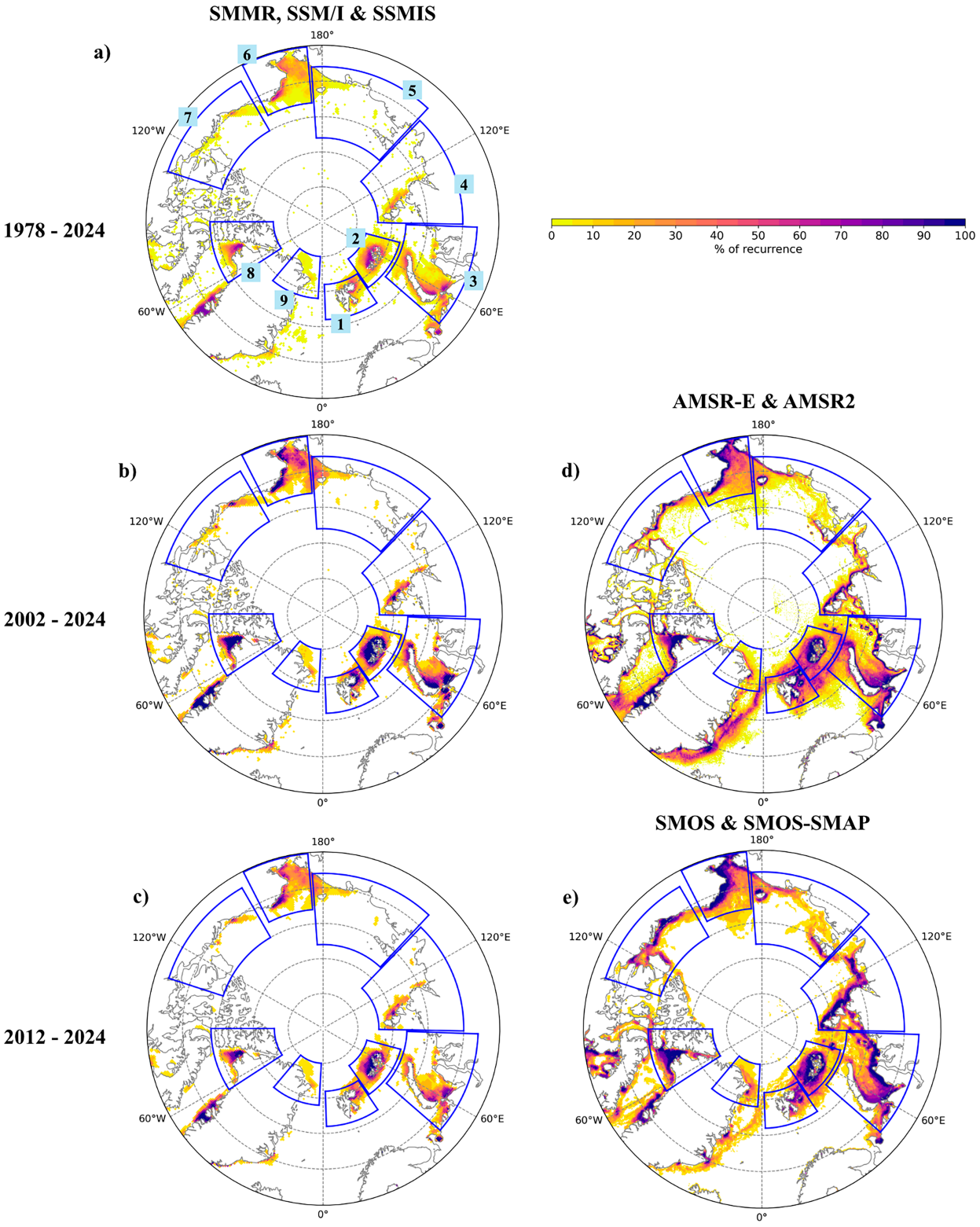

FIG. 3. Arctic polynya recurrence frequency for the three satellite datasets over their respective analysis period using a SIC threshold of 50% or SIT threshold of 20 cm. (a) SMMR, SSM/I & SSMIS have an analysis period of 1978–2024; (d) AMSR-E & AMSR2 have an analysis period of 2002–24; (e) SMOS & SMOS–SMAP have an analysis period of 2012–24. SMMR, SSM/I & SSMIS results over the same period as (b) AMSR-E & AMSR2 and (c) SMOS & SMOS–SMAP are also shown. Blue boxed regions in (a) indicate our regions of interest for the next section's analysis; their numbers match the regions in Table 3.

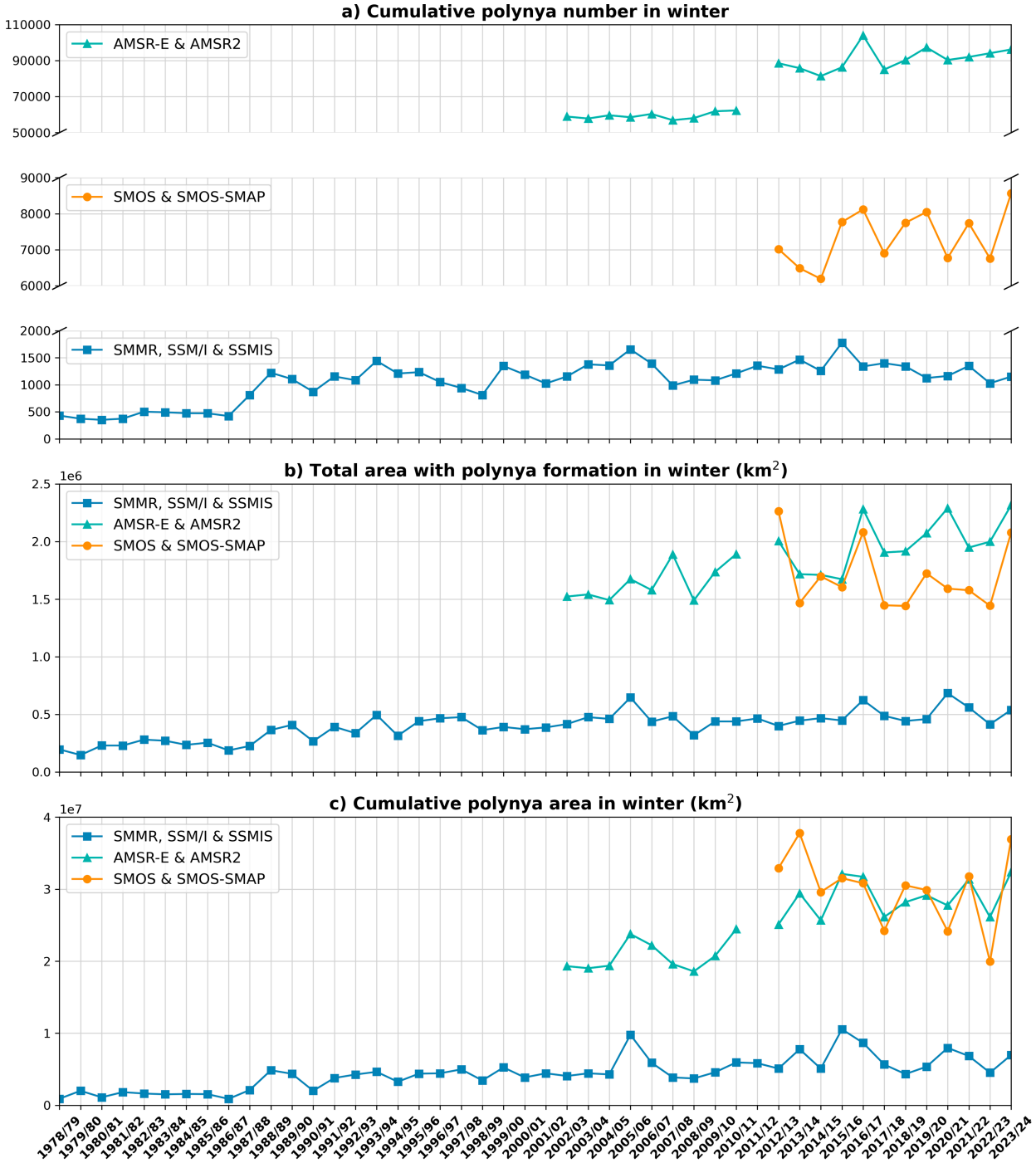

FIG. 4. (a) Cumulative polynya number, (b) total area with polynya formation, and (c) cumulative polynya area in winter (December–March) from 1978 to 2024 for the three different satellite products (colors, see section 2 for more details). Total polynya refers to area that has been identified as a polynya once in one winter, while cumulative area is the sum of daily polynya area in one winter. Note the broken *y* axis in (a) because of the different orders of magnitude for the products.

of 15%, yet the possibility remains that noise from the marginal ice zone (MIZ) is incorrectly identified as polynyas. There is a considerable uncertainty exceeding 10% in MIZ retrieval in satellite observation, according to Rolph et al. (2020), and thus, high-resolution data may overestimate polynya recurrence near the ice edge. There are some locations with high polynya formation signal but outside of the major polynya regions previously mentioned in the literature. For

TABLE 3. SMMR, SSM/I & SSMIS Arctic and regional winter polynya total area trend and cumulative area trends since 1978. All results are at or above the 90% statistical significance level, and "—" indicates that trends are under the significance level.

	Total polynya area trend (10^4 km^2 decade^{-1})			Cumulative polynya area trend (10^5 km^2 decade^{-1})		
Region	1978/79–2023/24	1978/79–2001/02 (period 1)	2002/03–2023/24 (period 2)	1978/79–2023/24	1978/79–2001/02 (period 1)	2002/03–2023/24 (period 2)
Arctic	7.08	11.0	—	5.79	8.31	—
1) Svalbard	—	—	—	0.23	0.33	—
2) Franz Josef Land	2.07	1.92	1.92	2.07	2.00	—
3) Kara Sea	1.08	3.24	—	0.87	1.96	—
4) Laptev Sea	0.66	—	—	0.25	—	—
5) East Siberian Sea	0.54	—	—	0.13	—	—
6) Chukchi Sea	1.67	4.12	2.43	0.48	1.67	1.16
7) Beaufort Sea	0.26	—	—	—	—	—
8) NOW	0.87	0.77	−1.37	1.00	0.77	—
9) NEW	0.18	—	—	—	—	—

example, at Disko Bay and Scoresby Sund in Greenland, the percentage of polynya recurrence also reaches over 50%; however, since these locations are close to the seasonal ice edge, we exclude these locations in our study to minimize the uncertainties induced by the MIZ.

The length of the satellite data period also influences the spatial patterns observed in Fig. 3. For SMMR, SSM/I & SSMIS, which has the longest SIC period (47 yr), locations with low (Fig. 3a, yellow–orange) and high recurrence (purple) are more distinguishable than for AMSR-E & AMSR2 (Fig. 3d) and SMOS & SMOS–SMAP (Fig. 3e). All three results show the major polynyas; however, in the Laptev Sea and the Kara Sea regions, the AMSR-E & AMSR2 and SMOS & SMOS–SMAP results show a higher percentage of recurrence (≥50%) along the entire coastline than SMMR, SSM/I & SSMIS. A similar situation can also be observed in the North East Water (NEW) and the East Siberian Sea. To facilitate comparison, we also produced a map using SMMR, SSM/I & SSMIS over the same time period as AMSR-E & AMSR2 (2002–24, Fig. 3b) and SMOS & SMOS–SMAP (2012–24, Fig. 3c). This shows the same result: The recurrence signal after the 2000s from the shortened SMMR, SSM/I & SSMIS (Figs. 3b,c) is stronger in the Laptev Sea, Kara Sea, and NEW than in the full time series (Fig. 3a). Despite the data resolution causing inconsistencies in the MIZ as mentioned above, this finding suggests that polynyas in those regions have occurred more frequently over the last two decades as AMSR-E & AMSR2 and SMOS & SMOS–SMAP satellite observations started after the 2000s. We, therefore, now conduct a temporal analysis of polynya activity.

b. *Temporal variability and trends in winter polynyas, at the pan-Arctic and regional scales*

The cumulative polynya number is inconsistent among the products (Fig. 4a). The cumulative polynya number from the 6.25-km resolution AMSR-E & AMSR2 is continuously exceeding 75 000 (Fig. 4a, turquoise). The SIT-based, 12.5-km resolution SMOS & SMOS–SMAP has a range of 6000–9000, constantly exceeding that of the SIC-based, 25-km resolution SMMR, SSM/I & SSMIS which fluctuates between 500 and 2000 over their common time period (Fig. 4a, orange and dark blue lines, respectively). This difference in the cumulative number caused by the resolution of the satellite products aligns with the differences in spatial distribution found in section 4a.

Both the total pan-Arctic winter polynya area and cumulative polynya area have an increasing trend for the past 47 years (Figs. 4b,c). The total area of polynyas calculated from AMSR-E & AMSR2 and SMOS & SMOS–SMAP is around double that from SMMR, SSM/I & SSMIS, and the cumulative area is nearly triple (Figs. 4b,c). It is logical that AMSR-E & AMSR2 and SMOS & SMOS–SMAP have larger area values than SMMR, SSM/I & SSMIS since more grid cells are identified as polynyas. Focusing on SMMR, SSM/I & SSMIS, which is the only time series with more than 20 years of uninterrupted results and, therefore, enhances the robustness of any trend analysis, we find a positive trend of 7.1×10^4 km^2 decade^{-1} for the total polynya area and 5.8×10^5 km^2 decade^{-1} for the cumulative area (Table 3). However, we find no significant trend in the polynya number; this indicates the regions where polynyas form and the extent of the polynyas have expanded over the past four decades.

From section 4a, we suspect that the more intense recurrence signal for the two more recent datasets is due to more active polynya formation after the 2000s. On a pan-Arctic scale, the total area has a positive trend of 11.0×10^4 km^2 decade^{-1} over 1978/79–2001/02, after which the trend disappears in 2002/03–2023/24. The cumulative area has a larger increase over 1978/79–2001/02 (8.3×10^5 km^2 decade^{-1}) than over 2002/03–2023/24 (no trend). These results suggest that the increase in both potential polynya location and area extent may have slowed down the same since the 2000s.

We hypothesize that the regional trends for the main polynyas may differ from each other based on our spatial findings (section 4a). We, therefore, define nine regions of interest based on our winter base map result where an intense recurrence signal was detected (Fig. 3), highlighted in Fig. 3a; their locations are stated in Table A1 in the appendix. Franz Josef Land (2.1×10^4 km^2 decade^{-1}), Chukchi Sea (1.7×10^3 km^2 decade^{-1}), and Kara Sea (1.1×10^3 km^2 decade^{-1}) have the largest

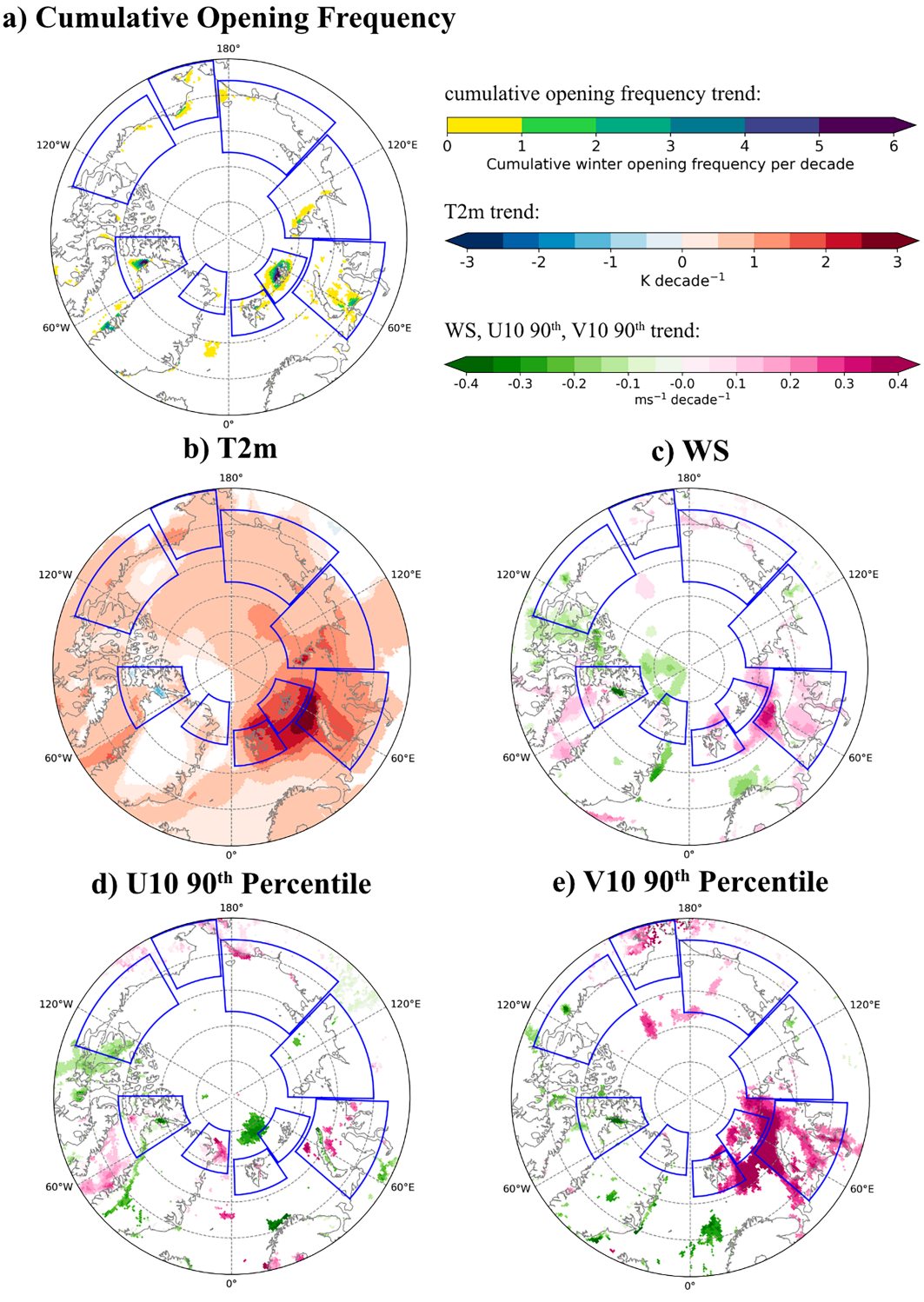

FIG. 5. The trend of (a) winter-cumulated opening frequency, (b) winter mean T2m, (c) winter mean WS, (d) winter mean U10 90th percentile, and (e) winter mean V10 90th percentile for 1978/79–2023/24. Positive (negative) values of U10 indicate wind direction toward the east (west), and positive (negative) values of V10 indicate wind direction toward the north (south). All results are at or above the 90% statistical significance level.

TABLE 4. Area-weighted winter mean trends of all atmospheric drivers. All results are at or above 90% statistically significant level.

Region	Area-weighted winter mean trend (1978/79–2023/24)			
	T2m (K decade^{-1})	WS (m s^{-1} decade^{-1})	U10 90th percentile (m s^{-1} decade^{-1})	V10 90th percentile (m s^{-1} decade^{-1})
Arctic	0.71	—	—	—
1) Svalbard	1.57	—	—	—
2) Franz Josef Land	1.85	—	—	—
3) Kara Sea	1.35	0.08	—	0.18
4) Laptev Sea	0.94	—	—	—
5) East Siberian Sea	0.68	—	—	—
6) Chukchi Sea	0.67	—	—	—
7) Beaufort Sea	0.61	—	—	—
8) NOW	0.37	—	—	—
9) NEW	0.39	—	—	—

increase in polynya area and contribute more than half of the increase in the pan-Arctic total polynya area trend (Table 3, see also Figs. A1 and A2 in the appendix). As discussed previously, in section 4a, we speculated that polynya formation is more active after the 2000s. Yet, when it comes to the trend differences over the two halves of the satellite record, only Franz Josef Land retains the same increasing rate in total polynya area over the period 2002/03–2023/24. For other regions such as the Kara Sea, Chukchi Sea, and North Open Water (NOW), the total polynya area trend is lower or even no longer significant between periods 1 and 2. Preußer et al. (2019) computed the average polynya area using a sea ice thickness threshold of 20 cm between 2002/03 and 2017/18, a similar time period to our period 2. Their increasing trend in area in Franz Josef Land (region 2) and Chukchi Sea (region 6) is consistent with our findings, albeit not directly comparable since they produced an average over the season. The other regions cannot be compared since Preußer et al. (2019) used different regional masks, but like us, they find regions with positive and others with negative trends. One region that featured in their study but not in ours is the Canadian Archipelago, in which they found a moderate increasing trend. It is also possible that the differences in significance are caused by the different time periods between our two studies, with trends disappearing when we added 6 years of data. Figures A1 and A2 in the appendix suggest a potential increase in the variability of polynya activity over period 2, which would be consistent with the observed increase of variability of the Arctic sea ice (Dörr et al. 2023). This would explain why trends are disappearing over period 2, but investigating this further is beyond the scope of this paper. In terms of the cumulative area, regions that contribute most to the trend are Franz Josef Land (2.1×10^5 km^2 decade^{-1}), NOW (1.0×10^5 km^2 decade^{-1}), and the Kara Sea (0.9×10^5 km^2 decade^{-1}); however, they do not have an accelerated positive trend in their second period unlike what we suspected from section 4a. We also find a decrease in the Chukchi Sea cumulative polynya area trend over the second period, and no trend exists in other regions after the 2000s.

Most polynya regions have an increase in their polynya opening frequency of 1–2 times per decade, whereas Franz Josef Land and NOW show a more evident increase of more than 6 times per decade (Fig. 5a). Regions with a higher cumulative opening frequency trend also have a positive trend in either temperature, wind, or both. For example, regions next to the Barents–Kara Sea have a significant increase in air temperature (T2m) of 1–3 K and WS of 0.1–0.3 m s^{-1} decade^{-1} (Figs. 5b,c). This is further shown in Table 4: The area-weighted mean T2m trend and recent studies have indicated that most Arctic regions have an increasing air temperature trend over the past few decades, especially for regions near the Atlantic Water inflow (e.g., Franz Josef Land; Kohnemann et al. 2017; Rantanen et al. 2022). The increasing air temperature trend also reveals that the warming atmosphere may be preconditioning the region for polynya opening by thinning the sea ice. Previous studies observed that sea ice transition begins around −20°C (Shupe et al. 2022). The yearly winter mean T2m of the Arctic for the past four decades is close to this threshold, and the yearly winter maximum T2m has even exceeded −20°C (Fig. A3). Arctic sea ice may be becoming easier to open by the wind in the warming Arctic. The area-weighted WS trend is not statistically significant in all regions except the Kara Sea. Looking at U10 and V10 at 90th percentile, an indicator for extreme wind activity crucial for dynamical forcings, there is a positive trend in the Kara Sea for U10 and V10. This strengthening of the southerly winds may be due to the higher frequency of winter extreme cyclone activity in the Eurasian sector in recent years (Rinke et al. 2017). Although area-weighted results do not show an evident trend for any of the wind variables in most regions, significant wind trends are present in some grid cells of the regions (Figs. 5c–e). In addition, the strong positive trend in southerly winds exceeding 0.4 m s^{-1} decade^{-1} locally over the Kara Sea may be leading to increased opening frequency in the north of neighboring Franz Josef Land (Figs. 5a,e). We present the full correlation analysis in section 4c to further investigate the relationship between these positive trends.

We finish the temporal analysis with an analysis of its monthly variability and whether this variability has changed as well. The maximum cumulative polynya area usually occurs in December or March at the pan-Arctic scale, but this varies across the different regions (Fig. 6). The area is maximal in early winter for regions on the Pacific side (East Siberian Sea, Chukchi Sea, and Beaufort Sea). For regions on the Atlantic

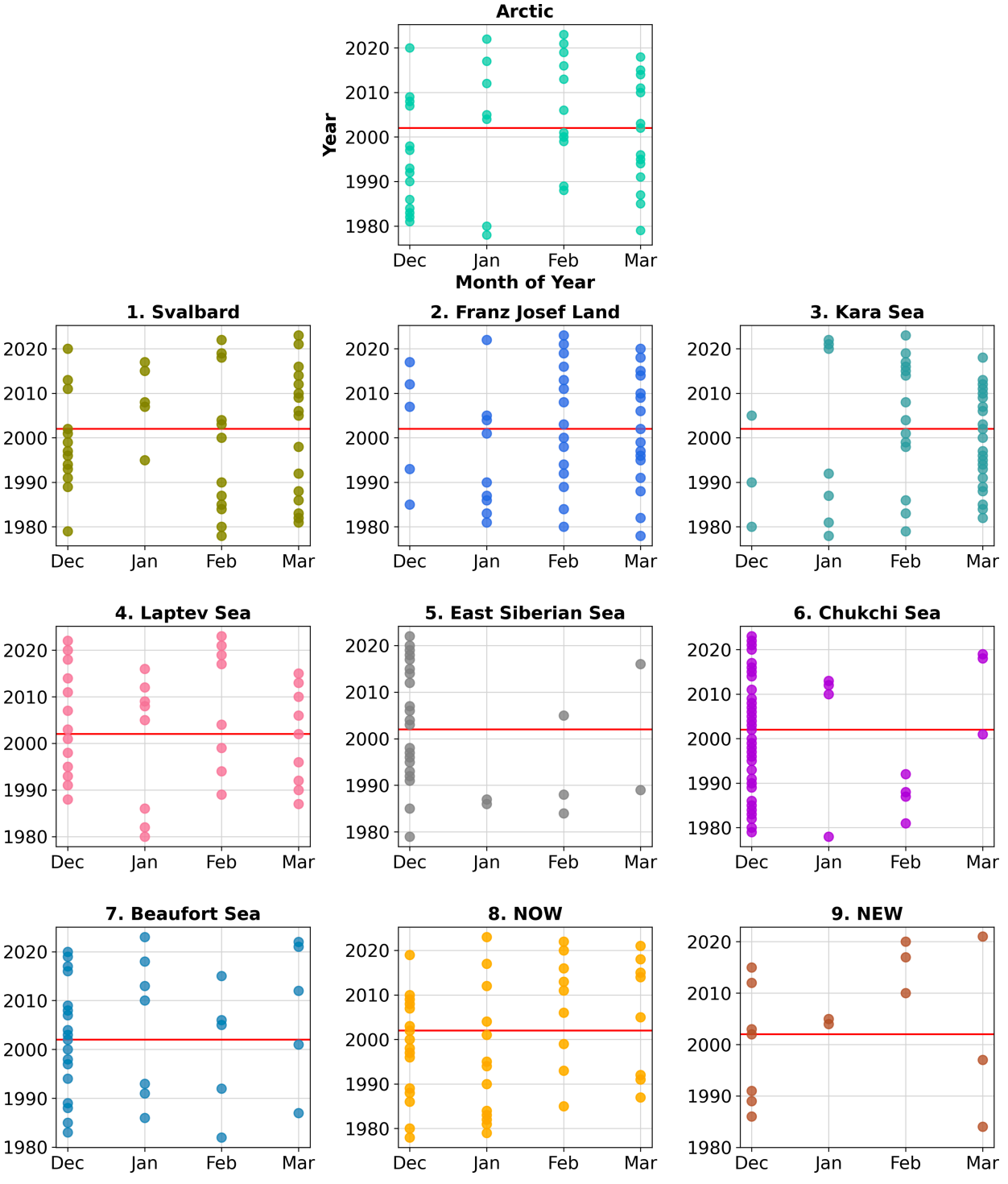

FIG. 6. The temporal distribution of the month of maximum cumulative polynya area from 1978 to 2024 for the Arctic and the various subregions. The red line is the year 2002, before and after which different trends in cumulative polynya area are calculated. One dot represents one winter if polynyas are formed during that winter period.

side (Svalbard, Franz Josef Land, Kara Sea, NEW), their maximum months are more widely spread but occur mainly in mid- or late winter. There has been a shift in the month of maximum area after the 2000s, but the direction of the shift depends on the region. Most noticeably, at the pan-Arctic scale, the maximum area is mainly found in either December or March in period 1, and yet, it becomes more evenly distributed within wintertime after 2002. At the subregional scale, the

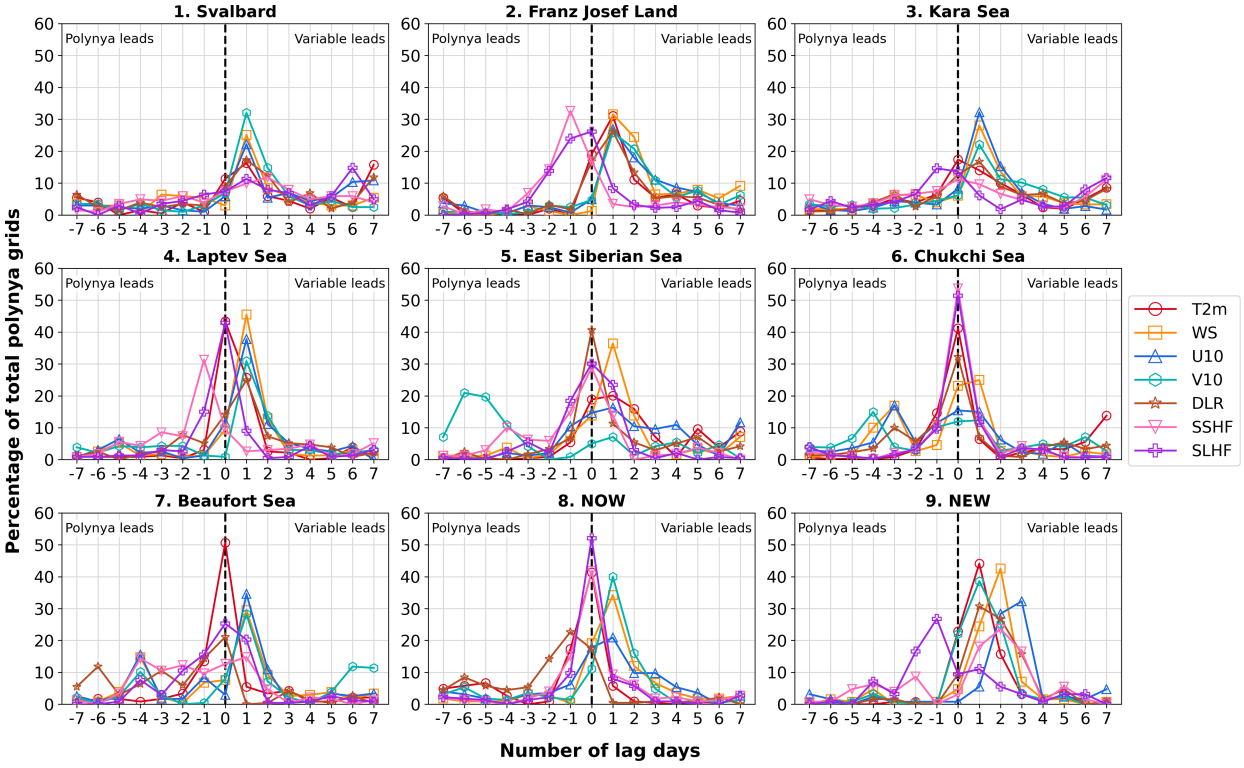

FIG. 7. Percentage of total polynya grids with maximum absolute correlation coefficient between the on–off polynya state and the potential atmospheric drivers and their respective fluxes: T2m in red; WS in orange; u and v component of wind U10 and V10 in dark blue and turquoise, respectively; DLR in brown; SSHF in pink; and SLHF in purple for the nine regions of interest. The x axis is the number of days of lag tested: Positive lag values mean before the polynya opens, i.e., the atmosphere leads; negative values means after the polynya opens, i.e., the polynya leads.

maximum area month consistently is December, with occasionally some other winter months, on the Pacific side; however, on the Atlantic side, it is clear that there is a maximum cumulative area month shift from period 1 to period 2. For example, in the NEW, the maximum cumulative area occurs in December or March in period 1, but it becomes 5 out of 10 in January and February in period 2. In Franz Josef Land and the Kara Sea, the maximum month is spread more evenly in period 1 but is now more concentrated in February or March in period 2.

The different shifts in seasonality and trends in different regions, despite an overall warming Arctic, suggest competing effects from the atmospheric drivers. We suspect that there may be a correlation between polynya events and atmospheric conditions; however, it is difficult to quantify the effect of the atmosphere on a winter-averaged time scale. Therefore, in the next section, we will examine the correlation from a daily scale perspective.

c. *Atmospheric forcings on polynya openings*

We conduct a lagged correlation analysis between the on–off polynya state and the time series of the four potential drivers at the same location (air temperature in red, wind speed in orange, and u and v winds in dark blue and turquoise, respectively, in Fig. 7), as well as three fluxes to better distinguish the relative role of temperature and wind (DLR in brown, SSHF in pink, SLHF in purple in Fig. 7). For each lag, we determine the percentage of grid cells where the correlation is maximal for that lag in each region. Positive lag values (to the right) are days before the polynya opens; negative lag values (to the left) are after the polynya has opened. In half of the regions (Svalbard, Franz Josef Land, East Siberian Sea, and NEW), all atmospheric variables, i.e., both wind and temperature, have a maximum correlation 1–2 days prior to the openings (red, orange, blue, and turquoise lines on day 1/2 in Fig. 7). If they are drivers for the opening, DLR, SSHF, and SLHF would have the highest correlation on day 0 for their overlaying effect. In the East Siberian Sea, DLR (brown line), SSHF (pink line), and SLHF (purple line) indeed peak on day 0, suggesting that both temperature and wind may have an impact on the polynya opening. In Franz Josef Land, only SLHF peaks on day 0, while SSHF is lagged by −1 day. This may be a signal that wind triggers the Franz Josef Land polynyas to open, which increases upward latent heat flux instantaneously. The T2m may have some preconditioning effect on the opening by thinning the ice, but the opening happens due to the wind. The opening enhances the local temperature and downwelling radiation, which would explain the SSHF peak on day −1. Svalbard and NEW do not show this distinct high correlation of the fluxes on day 0. Instead, SSHF peaks 2 days

TABLE 5. Lagged correlation between potential drivers and daily polynya area, with atmospheric variables (polynya areas) first on positive (negative) lag days. All results are at or above the 90% statistical significance level. Full lagged correlation tables can be found in Tables A2–A5 in the appendix. Correlation with the fluxes is in the next table.

	T2m			WS			U10 90th percentile			V10 90th percentile		
Region	Day −1	Day 0	Day 1	Day −1	Day 0	Day 1	Day −1	Day 0	Day 1	Day −1	Day 0	Day 1
Arctic	0.25	0.25	0.24	0.09	0.15	0.19	0.10	0.12	0.12	0.10	0.16	0.20
1) Svalbard	0.05	0.05	0.06	−0.03	—	0.03	0.06	0.08	0.09	—	—	—
2) Franz Josef Land	0.36	0.42	0.43	0.18	0.29	0.36	−0.03	−0.03	−0.03	0.16	0.25	0.33
3) Kara Sea	0.25	0.27	0.26	0.11	0.18	0.22	0.08	0.10	0.10	0.07	0.12	0.14
4) Laptev Sea	0.17	0.19	0.19	0.11	0.18	0.21	0.11	0.17	0.19	0.08	0.11	0.15
5) East Siberian Sea	0.05	0.06	0.07	0.05	0.06	0.05	−0.04	−0.03	−0.03	—	—	—
6) Chukchi Sea	0.14	0.16	0.15	0.11	0.15	0.16	−0.06	−0.07	−0.07	—	0.04	0.04
7) Beaufort Sea	0.07	0.07	0.05	—	0.05	0.06	—	—	−0.03	0.04	0.08	0.07
8) NOW	0.24	0.24	0.21	0.17	0.33	0.32	—	0.09	0.09	—	−0.09	−0.17
9) NEW	0.11	0.14	0.14	0.03	0.06	0.07	—	−0.04	−0.07	0.11	0.18	0.20

before the opening in these two regions. Along with the stronger correlation for V10, this suggests that the warm southerly winds are the main drivers in these two regions. In the other regions (Kara Sea, Laptev Sea, Chukchi Sea, Beaufort Sea, and NOW), all wind variables have a maximum correlation 1 day before polynya opening, and SLHF peaks on day 0 or day −1, i.e., after the opening, suggesting that these are most likely traditional latent heat polynyas. The significant instantaneous correlation of T2m may be explained as the instantaneous effect of polynya opening on the local atmosphere, consistent with the increase in SSHF.

The radiative fluxes also suggest a delayed effect of polynya openings on the atmosphere. In some regions, for example, Franz Josef Land and the Beaufort Sea, the high SSHF and SLHF correlations can last for 2–3 days after the opening. Feedback effects on the wind, suggested by the increasing correlations several days after the opening (orange, blue, and turquoise lines in the East Siberian Sea, Chukchi Sea, and Beaufort Sea in Fig. 7), are beyond the scope of this paper but would be worth investigating further, for example, using model simulations.

Besides the polynya state, we also determine the relationship between polynya area and its potential atmospheric drivers, including the longwave radiation and sensible and latent heat fluxes, to try and detangle the contribution of temperature and wind. The correlation values are listed in Tables 5 and 6, limiting our results to day −1, day 0, and day 1 only since we found the lag effect to be the most prominent 1 day before and after the opening (Fig. 7). The T2m is more positively correlated to the daily total polynya area than WS in all regions. From a pan-Arctic perspective, the correlation with T2m is higher than those of any wind parameter, regardless of the lag (Tables 5 and A2). The correlation of T2m reaches up to 0.24 on lagged day 1 on a pan-Arctic scale but only 0.2 for V10 90th percentile, which is consistent with the higher correlation for DLR than for the other fluxes on days −1 and 0. As expected, the correlations vary between the regions though. There is a relatively stronger correlation between T2m and WS with daily polynya ($R > 0.2$) in Franz Josef Land and NOW than in other regions on lag day 1 (Table 5). The U10 and V10 90th percentile correlations are smaller than T2m and WS in general, but in Franz Josef Land, the V10 90th percentile correlation is similar to the WS correlation. This may suggest that the effect of V10, the meridional wind, is significant in polynya area extent at the Franz Josef Land, as we suspect for the neighboring Svalbard region from the lagged analysis. The importance of the air temperature is also visible from the correlation for DLR on day −1 and day 0. Most of the regions have low

TABLE 6. Lagged correlation between the daily polynya area and the DLR, SSHF, and SLHF, with flux variables (polynya areas) first on positive (negative) lag days. All results are at or above the 90% statistical significance level. Full lagged correlation tables can be found in Tables A6–A8 in the appendix.

	DLR			SSHF			SLHF		
Region	Day −1	Day 0	Day 1	Day −1	Day 0	Day 1	Day −1	Day 0	Day 1
Arctic	0.26	0.27	0.25	0.09	0.10	0.10	—	—	−0.02
1) Svalbard	0.06	0.05	0.06	—	—	—	—	—	—
2) Franz Josef Land	0.30	0.36	0.38	−0.16	−0.07	—	−0.31	−0.27	−0.21
3) Kara Sea	0.22	0.25	0.24	0.11	0.15	0.17	0.04	0.06	0.07
4) Laptev Sea	0.14	0.16	0.17	—	0.10	0.15	−0.19	−0.19	−0.15
5) East Siberian Sea	0.03	0.05	0.05	−0.03	−0.03	—	−0.17	−0.20	−0.19
6) Chukchi Sea	0.12	0.14	0.12	−0.18	−0.16	−0.15	−0.27	−0.29	−0.28
7) Beaufort Sea	0.05	0.04	—	—	—	—	−0.15	−0.18	−0.17
8) NOW	0.19	0.15	0.10	−0.16	−0.09	−0.03	−0.51	−0.58	−0.48
9) NEW	0.04	0.07	0.08	0.05	0.10	0.13	−0.09	−0.07	−0.04

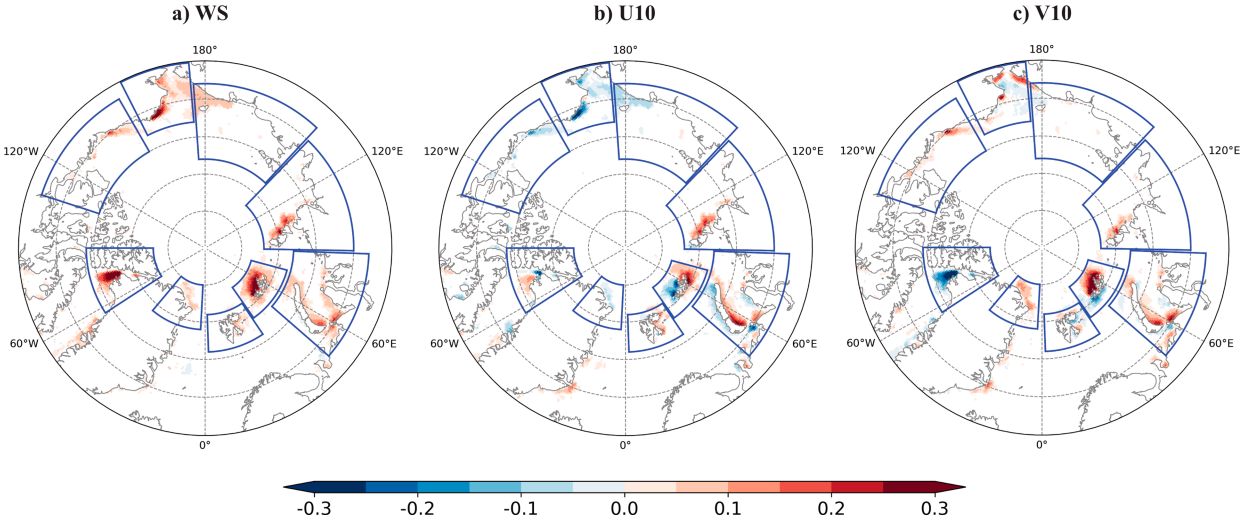

FIG. 8. The 1-day-lag correlation of on–off state with daily (a) WS, (b) U10, and (c) V10. Colored areas are at or above the 90% significance level. The U10 is positive toward the east, and V10 is positive toward the north.

correlation values with SSHF ($R < 0.15$) but more evident correlation values with SLHF ($R > 0.15$), implying most of them are latent heat polynyas (Table 6). To summarize, our results suggest that wind is crucial for opening the polynyas, most of which are latent heat polynyas, although in half the regions, the air temperature plays a preconditioning effect. But once the polynya is open, air temperature is essential to maintain the polynya extent. The role of the ocean in maintaining the polynya can unfortunately not be assessed due to a lack of observations.

Finally, since we found in Fig. 7 that in all regions it is not only the strength of wind that matters but also the wind direction, we finish with a spatial analysis of the wind speed and direction's correlation, with a 1-day lag. We again find a positive correlation between polynya opening and the previous day's wind speed (Fig. 8a) for most of the major polynyas, with $R \geq 0.3$. For regions with a high WS correlation, most polynya openings align with the wind direction from the continent to the Arctic region, as shown by the correlation with the two wind components (Figs. 8b,c): Polynyas formed in the Barents–Kara Sea mainly correlate with both U10 and V10 (wind from the Eurasian continent), while on the side of the Chukchi Sea, they correlate with U10 only (eastward wind along the Canadian archipelago). In NOW, where winds flow parallel to the Nares Strait due to the channeling effect of the local topography, polynya activity is more strongly correlated with V10 (correlations exceeding -0.3); a negative value means that polynya openings are associated with stronger southerly winds or weaker northerly ones. Franz Josef Land is the only region where all three wind parameters have a high correlation (Fig. 8). The dipoles in correlations (Figs. 8b,c), negative in the south or west and positive in the north or east, are consistent with findings from, e.g., Tamura and Ohshima (2011) and Preußer et al. (2015) who showed enhanced ice production in the lee of the islands. Although the wind in the region showed no trend (Table 4), it did in the neighboring Kara Sea, which may explain the strong increase in polynya area around Franz Josef Land. The Chukchi Sea region is more correlated with U10, while NOW is more correlated with V10. From Fig. 5, the increasing opening trend in NOW aligns with the stronger northerly wind along the Nares Strait, whereas the weak opening frequency trend in the Chukchi Sea may be implied by the absence of wind trends in that area. Combining all our findings, we can conclude that in agreement with past studies, wind plays a significant role in the opening of most Arctic polynyas, and that the inconsistent trends in space and time of the winds is the reason for the complex, nonlinear polynya trends we quantified.

5. Conclusions

The main purpose of this study was to examine the spatial and temporal distributions of most Arctic polynyas that occurred in the past 47 years, with existing passive microwave satellite sea ice products. We also quantified the correlation between polynya events and atmospheric variables. Our main findings can be summarized as follows:

- Regardless of the sea ice product, the regions with the highest polynya recurrence are the western Laptev Sea, the western Kara Sea, Franz Josef Land, eastern Svalbard, North Open Water, and the Chukchi Sea. The detected polynya area and polynya numbers are affected by the product's horizontal resolution, with high resolution resulting in noise in the marginal ice zone. For now, the short time coverage and uncertainty in the data product limit the usefulness of the sea ice thickness retrievals.
- Both the total and cumulative winter polynya areas have an increasing trend in the Arctic of approximately 71 000 and 580 000 km^2 decade^{-1}, respectively, over 1978–2024. Total winter polynya area is dominated by trends in Franz Josef Land, the Chukchi Sea, and the Kara Sea, whereas the cumulative area is more influenced by trends in Franz Josef Land, NOW, and the Kara Sea.

- The correlation analysis indicates that wind speed and direction are most related to the opening of a polynya, up to 2 days prior to opening; sensible and latent heat fluxes confirm that most polynyas in the Arctic are latent heat polynyas. The air temperature also has a large correlation with opening in half the regions, suggesting an important preconditioning role of the temperature (which is also suggested by the longwave downward radiation). Temperature is, however, most correlated with the polynya area, after the opening.

Our results suggest that polynya activity will increase further as air temperatures continue to rise and extreme wind events become more frequent, particularly in some regions that already have a high recurrence signal of polynyas (Fig. 5a). We acknowledge that the correlation coefficients, although significant, are not large (Tables 5, 6, and A2–A8), showing that polynyas are a complex natural phenomenon resulting from the interplay of geography, preconditioning, and triggering. Moreover, the lack of observations in the Arctic Ocean means that we have to assume but cannot confirm that the ocean is fully mixed and, therefore, not contributing to the preconditioning. As winter Arctic sea ice cover continues to decrease (Cavalieri and Parkinson 2012), the number of Arctic polynya may be reduced due to sea ice retreat or may soon extend to the open ocean where they would be affected by different drivers, both in the atmosphere and the ocean; their study might, however, become even more complex owing to data paucity in the open Arctic Ocean. Yet, understanding the drivers and impacts of polynyas is not only beneficial for understanding their local effects on the climate but also a prerequisite for accurate monitoring and projections of local biological activity, pan-Arctic air–sea exchanges of carbon and oxygen, and the global oceanic circulation.

Acknowledgments. This work was funded by the Swedish National Space Agency Grant 2022-00149 awarded to CH. The computations were enabled by resources provided by the National Academic Infrastructure for Supercomputing in Sweden (NAISS), partially funded by the Swedish Research Council through Grant Agreement 2022-06725. We thank the three anonymous reviewers and the editor Qinghua Ding for their comments that improved the quality of this manuscript.

Data availability statement. The script for the polynya retrieval algorithm, using NSIDC SIC data as an example, is available on GitHub at https://github.com/carmenwhm/Arctic_polynyas_paper.git. The observed sea ice concentration data from the NSIDC are available at https://nsidc.org/data/nsidc-0051/versions/2, last accessed on 24 April 2025. The observed sea ice concentration and sea ice thickness data from the University of Bremen Sea Ice Remote Sensing group are available at https://seaice.uni-bremen.de/start/, last accessed on 24 April 2025. Fifth generation European Centre for Medium-Range Weather Forecasts atmospheric reanalysis (ERA5) hourly data on single levels are available at https://cds.climate.copernicus.eu/datasets/reanalysis-era5-single-levels?tab=download, last accessed on 22 September 2025. The daily polynya masks produced from SMMR, SSM/I & SSMIS and SMOS & SMOS-SMAP are publicly available on PANGAEA at https://doi.org/10.1594/PANGAEA.987383.

APPENDIX

Full Regional Analysis Results

Figures A1 and A2 show the regional total area with polynya formation and cumulative daily area with polynya formation in winter during 1978–2024, respectively. Figure A3 presents a scattered boxplot of the yearly winter mean T2m and yearly winter maximum T2m for Arctic and all regions. Table A1 lists the spatial information of the nine regions of interest. Tables A2–A8 present the full lag correlation results of meteorological variables and daily polynya area.

FIG. A1. Regional total area with polynya formation in winter (December–March) from 1978 to 2024. Orange lines show the area trend with above 90% significance.

FIG. A2. Regional cumulative daily area with polynya formation in winter (December–March) from 1978 to 2024. Orange lines show the area trend with above 90% significance.

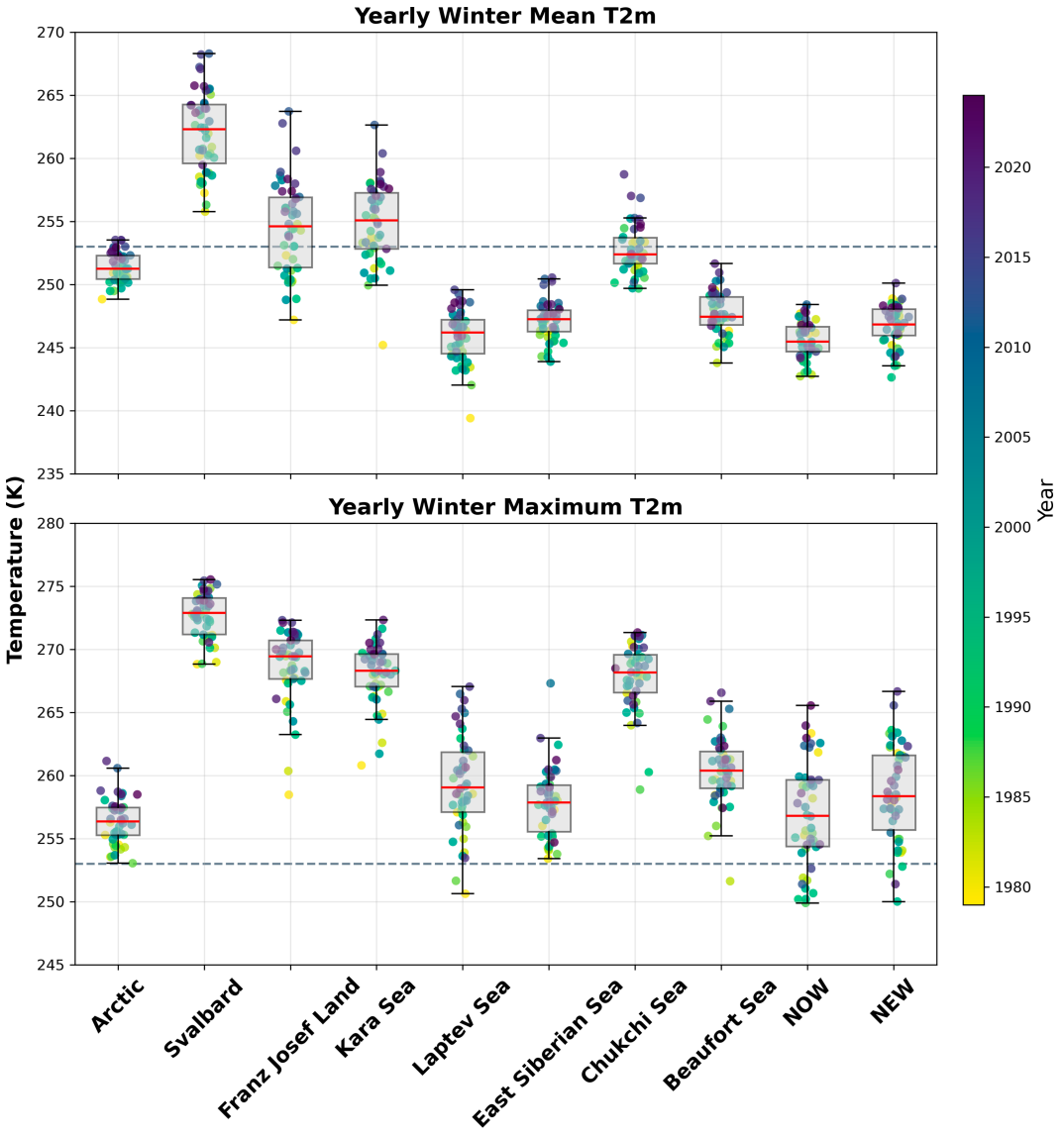

FIG. A3. Scattered boxplot of the (top) yearly winter mean T2m and (bottom) yearly winter maximum T2m for Arctic and all regions. One dot represents the winter mean or maximum of one winter from 1978/79 to 2023/24. Red lines present the median of the mean/maximum distribution. Dotted lines refer to a temperature of 253 K, which is equivalent to −20°C when sea ice transition occurs during MOSAIC (Shupe et al. 2022).

TABLE A1. Spatial information of the nine regions of interest for the lag correlation analysis.

Region	Lat, lon
1) Svalbard	76°–81°N, 2°–34°E
2) Franz Josef Land	78.5°–83.5°N, 35°–73°E
3) Kara Sea	68°–78°N, 49°–88°E
4) Laptev Sea	70°–82°N, 89°–136°E
5) East Siberian Sea	68°–78°N, 137°E–176°W
6) Chukchi Sea	65°–73°N, 153°–175°W
7) Beaufort Sea	67°–75°N, 108°–150°W
8) NOW	74°–83°N, 57°–90°W
9) NEW	79°–85°N, 3°–40°W

TABLE A2. Lag correlation results of T2m with daily polynya area. All results are at or above the 90% statistical significance level.

	Day														
Region	−7	−6	−5	−4	−3	−2	−1	0	1	2	3	4	5	6	7
Arctic	0.19	0.20	0.21	0.22	0.23	0.24	0.25	0.25	0.24	0.23	0.21	0.19	0.18	0.17	0.16
1) Svalbard	—	0.03	0.03	0.03	0.04	0.05	0.05	0.05	0.06	0.05	0.04	0.03	0.03	—	—
2) Franz Josef Land	0.20	0.21	0.21	0.23	0.26	0.30	0.36	0.42	0.43	0.40	0.36	0.32	0.29	0.26	0.24
3) Kara Sea	0.13	0.14	0.15	0.17	0.19	0.22	0.25	0.27	0.26	0.23	0.20	0.18	0.15	0.12	0.11
4) Laptev Sea	0.11	0.12	0.12	0.12	0.13	0.14	0.17	0.19	0.19	0.17	0.15	0.13	0.12	0.11	0.10
5) East Siberian Sea	—	—	—	—	0.03	0.04	0.05	0.06	0.07	0.06	0.06	0.06	0.06	0.06	0.06
6) Chukchi Sea	0.06	0.07	0.08	0.09	0.10	0.12	0.14	0.16	0.15	0.13	0.12	0.11	0.11	0.11	0.11
7) Beaufort Sea	0.03	0.03	0.04	0.04	0.05	0.06	0.07	0.07	0.05	0.04	0.04	0.03	0.03	0.03	0.04
8) NOW	0.11	0.13	0.16	0.18	0.20	0.23	0.24	0.24	0.21	0.18	0.16	0.15	0.14	0.13	0.12
9) NEW	—	0.03	0.04	0.05	0.07	0.08	0.11	0.14	0.14	0.14	0.13	0.12	0.11	0.09	0.08

TABLE A3. Lag correlation results of WS with daily polynya area. All results are at or above the 90% statistical significance level.

	Day														
Region	−7	−6	−5	−4	−3	−2	−1	0	1	2	3	4	5	6	7
Arctic	—	—	—	—	—	0.05	0.09	0.15	0.19	0.17	0.14	0.11	0.08	0.05	0.04
1) Svalbard	−0.02	—	—	—	—	−0.03	−0.03	—	0.03	0.03	—	—	—	—	—
2) Franz Josef Land	0.04	0.04	0.04	0.06	0.07	0.11	0.18	0.29	0.36	0.33	0.27	0.21	0.16	0.13	0.12
3) Kara Sea	—	—	—	—	0.03	0.05	0.11	0.18	0.22	0.20	0.17	0.12	0.07	0.04	—
4) Laptev Sea	0.04	0.05	0.06	0.05	0.05	0.07	0.11	0.18	0.21	0.19	0.15	0.11	0.08	0.06	0.06
5) East Siberian Sea	0.04	0.04	0.03	0.04	0.04	0.05	0.05	0.06	0.05	0.03	0.03	0.02	—	—	—
6) Chukchi Sea	0.07	0.06	0.06	0.07	0.08	0.09	0.11	0.15	0.16	0.14	0.11	0.08	0.05	0.03	—
7) Beaufort Sea	—	—	—	0.03	0.03	—	—	0.05	0.06	0.04	—	—	—	—	—
8) NOW	0.02	0.03	0.04	0.05	0.07	0.09	0.17	0.33	0.32	0.23	0.18	0.13	0.08	0.05	0.04
9) NEW	−0.03	−0.03	—	—	—	—	0.03	0.06	0.07	0.07	0.05	0.03	—	—	—

TABLE A4. Lag correlation results of U10 90th percentile with daily polynya area. All results are at or above the 90% statistical significance level.

	Day														
Region	−7	−6	−5	−4	−3	−2	−1	0	1	2	3	4	5	6	7
Arctic	—	—	—	—	—	0.05	0.10	0.12	0.12	0.12	0.12	0.11	0.10	0.08	0.07
1) Svalbard	—	—	—	—	—	0.04	0.06	0.08	0.09	0.09	0.08	0.07	0.08	0.08	0.07
2) Franz Josef Land	—	—	—	—	−0.03	−0.03	−0.03	−0.03	−0.03	—	—	—	0.03	0.03	—
3) Kara Sea	—	—	—	—	0.03	0.05	0.08	0.10	0.10	0.10	0.10	0.07	0.05	0.03	—
4) Laptev Sea	0.04	0.05	0.06	0.05	0.05	0.07	0.11	0.18	0.21	0.19	0.15	0.11	0.08	0.06	0.06
5) East Siberian Sea	−0.02	−0.04	−0.04	−0.04	−0.04	−0.05	−0.04	−0.03	−0.03	−0.03	—	—	−0.03	−0.03	—
6) Chukchi Sea	—	—	−0.02	−0.03	−0.04	−0.05	−0.06	−0.07	−0.07	−0.06	−0.04	−0.05	−0.04	—	—
7) Beaufort Sea	—	—	—	—	0.02	—	—	—	−0.03	−0.03	—	—	—	—	—
8) NOW	—	0.03	0.03	—	—	—	—	0.09	0.09	0.06	0.04	0.03	0.02	—	—
9) NEW	—	—	—	—	0.03	—	—	−0.04	−0.07	−0.08	−0.08	−0.06	−0.04	−0.03	−0.02

TABLE A5. Lag correlation results of V10 90th percentile with daily polynya area. All results are at or above the 90% statistical significance level.

	Day														
Region	−7	−6	−5	−4	−3	−2	−1	0	1	2	3	4	5	6	7
Arctic	—	—	—	—	0.03	0.06	0.10	0.16	0.20	0.21	0.19	0.17	0.15	0.13	0.11
1) Svalbard	—	—	−0.03	—	—	—	—	—	—	—	—	—	—	—	—
2) Franz Josef Land	0.03	0.03	0.03	0.04	0.06	0.10	0.16	0.25	0.33	0.34	0.32	0.28	0.24	0.21	0.20
3) Kara Sea	—	—	—	—	0.03	0.05	0.07	0.12	0.14	0.15	0.14	0.12	0.10	0.08	0.06
4) Laptev Sea	0.03	0.03	0.04	0.05	0.05	0.06	0.08	0.11	0.15	0.15	0.13	0.10	0.08	0.07	0.08
5) East Siberian Sea	−0.07	−0.06	−0.05	−0.03	−0.03	−0.02	—	—	—	—	—	—	—	—	—
6) Chukchi Sea	—	—	—	—	—	—	—	0.04	0.04	—	—	—	—	—	—
7) Beaufort Sea	—	—	—	—	—	—	0.04	0.08	0.07	0.04	—	—	—	—	—
8) NOW	—	—	—	—	0.02	—	—	−0.09	−0.17	−0.16	−0.12	−0.09	−0.08	−0.05	−0.05
9) NEW	—	—	—	—	0.02	0.06	0.11	0.18	0.20	0.18	0.16	0.13	0.11	0.09	0.08

TABLE A6. Lag correlation results of DLR with daily polynya area. All results are at or above the 90% statistical significance level.

	Day														
Region	−7	−6	−5	−4	−3	−2	−1	0	1	2	3	4	5	6	7
Arctic	0.19	0.20	0.21	0.22	0.23	0.24	0.26	0.27	0.25	0.24	0.22	0.20	0.19	0.17	0.15
1) Svalbard	0.04	0.04	0.04	0.05	0.05	0.05	0.06	0.05	0.06	0.05	0.05	0.04	0.03	—	0.02
2) Franz Josef Land	0.16	0.16	0.16	0.17	0.20	0.24	0.30	0.36	0.38	0.35	0.32	0.28	0.25	0.23	0.21
3) Kara Sea	0.12	0.13	0.14	0.16	0.18	0.20	0.22	0.25	0.24	0.22	0.19	0.17	0.15	0.12	0.11
4) Laptev Sea	0.10	0.11	0.11	0.11	0.11	0.12	0.14	0.16	0.17	0.16	0.15	0.13	0.11	0.09	0.08
5) East Siberian Sea	—	—	—	—	—	0.03	0.03	0.05	0.05	0.05	0.06	0.06	0.06	0.05	0.06
6) Chukchi Sea	0.06	0.06	0.07	0.08	0.09	0.10	0.12	0.14	0.12	0.10	0.09	0.08	0.07	0.07	0.07
7) Beaufort Sea	0.03	0.03	0.03	0.03	0.04	0.04	0.05	0.04	—	—	—	—	—	—	—
8) NOW	0.09	0.10	0.12	0.14	0.16	0.18	0.19	0.15	0.10	0.08	0.08	0.08	0.09	0.09	0.09
9) NEW	—	—	—	—	—	—	0.04	0.07	0.08	0.09	0.09	0.08	0.07	0.05	0.05

TABLE A7. Lag correlation results of SSHF with daily polynya area. All results are at or above the 90% statistical significance level.

	Day														
Region	−7	−6	−5	−4	−3	−2	−1	0	1	2	3	4	5	6	7
Arctic	0.05	0.06	0.06	0.05	0.06	0.07	0.09	0.10	0.10	0.10	0.11	0.12	0.12	0.12	0.11
1) Svalbard	—	—	—	—	—	—	—	—	—	—	−0.02	−0.03	—	−0.03	—
2) Franz Josef Land	−0.07	−0.10	−0.13	−0.16	−0.18	−0.18	−0.16	−0.07	—	0.07	0.08	0.07	0.06	0.05	0.03
3) Kara Sea	0.03	0.03	0.04	0.05	0.07	0.09	0.11	0.15	0.17	0.17	0.16	0.15	0.13	0.11	0.10
4) Laptev Sea	—	—	—	—	—	—	—	0.10	0.15	0.14	0.12	0.09	0.08	0.07	0.08
5) East Siberian Sea	−0.05	−0.04	−0.04	−0.03	−0.03	−0.03	−0.03	−0.03	—	—	—	—	—	−0.02	−0.03
6) Chukchi Sea	−0.06	−0.08	−0.11	−0.14	−0.16	−0.17	−0.18	−0.16	−0.15	−0.15	−0.16	−0.15	−0.12	−0.11	−0.09
7) Beaufort Sea	−0.03	−0.03	−0.03	−0.03	−0.03	−0.03	—	—	—	—	—	—	—	−0.03	−0.03
8) NOW	−0.08	−0.10	−0.10	−0.11	−0.12	−0.15	−0.16	−0.09	−0.03	—	—	—	—	—	—
9) NEW	−0.03	−0.03	—	—	—	0.03	0.05	0.10	0.13	0.13	0.11	0.09	0.08	0.07	0.06

TABLE A8. Lag correlation results of SLHF with daily polynya area. All results are at or above the 90% statistical significance level.

Region	Day														
	−7	−6	−5	−4	−3	−2	−1	0	1	2	3	4	5	6	7
Arctic	—	—	—	—	—	—	—	—	−0.02	—	—	0.03	0.05	0.05	0.05
1) Svalbard	—	—	—	—	—	—	—	—	—	−0.02	−0.03	−0.04	−0.03	−0.04	—
2) Franz Josef Land	−0.16	−0.18	−0.21	−0.25	−0.28	−0.30	−0.31	−0.27	−0.21	−0.16	−0.12	−0.10	−0.08	−0.08	−0.08
3) Kara Sea	—	—	—	0.02	0.03	0.04	0.04	0.06	0.07	0.07	0.08	0.09	0.09	0.08	0.08
4) Laptev Sea	−0.06	−0.08	−0.09	−0.10	−0.11	−0.14	−0.19	−0.19	−0.15	−0.10	−0.06	−0.03	−0.03	−0.03	−0.03
5) East Siberian Sea	−0.06	−0.07	−0.08	−0.10	−0.12	−0.14	−0.17	−0.20	−0.19	−0.17	−0.15	−0.11	−0.09	−0.08	−0.08
6) Chukchi Sea	−0.10	−0.12	−0.14	−0.18	−0.21	−0.23	−0.27	−0.29	−0.28	−0.26	−0.25	−0.24	−0.20	−0.18	−0.16
7) Beaufort Sea	−0.04	−0.07	−0.09	−0.10	−0.12	−0.14	−0.15	−0.18	−0.17	−0.14	−0.10	−0.08	−0.06	−0.05	−0.06
8) NOW	−0.17	−0.20	−0.23	−0.27	−0.32	−0.40	−0.51	−0.58	−0.48	−0.36	−0.27	−0.21	−0.15	−0.12	−0.10
9) NEW	—	—	−0.03	−0.04	−0.06	−0.09	−0.09	−0.07	−0.04	—	—	0.05	0.05	0.05	0.06

REFERENCES

Aagaard, K., L. K. Coachman, and E. Carmack, 1981: On the halocline of the Arctic Ocean. *Deep-Sea Res.*, **28A**, 529–545, https://doi.org/10.1016/0198-0149(81)90115-1.

Adams, S., S. Willmes, D. Schröder, G. Heinemann, M. Bauer, and T. Krumpen, 2013: Improvement and sensitivity analysis of thermal thin-ice thickness retrievals. *IEEE Trans. Geosci. Remote Sens.*, **51**, 3306–3318, https://doi.org/10.1109/TGRS.2012.2219539.

Bailey, D. A., A. H. Lynch, and T. E. Arbetter, 2004: Relationship between synoptic forcing and polynya formation in the Cosmonaut Sea: 2. Regional climate model simulations. *J. Geophys. Res.*, **109**, C04023, https://doi.org/10.1029/2003jc001838.

Bareiss, J., and K. Görgen, 2005: Spatial and temporal variability of sea ice in the Laptev Sea: Analyses and review of satellite passive-microwave data and model results, 1979 to 2002. *Global Planet. Change*, **48**, 28–54, https://doi.org/10.1016/j.gloplacha.2004.12.004.

Bennett, M. G., I. A. Renfrew, D. P. Stevens, and G. W. K. Moore, 2024: The Northeast Water Polynya, Greenland: Climatology, atmospheric forcing and ocean response. *J. Geophys. Res. Oceans*, **129**, e2023JC020513, https://doi.org/10.1029/2023JC020513.

Boisvert, L. N., T. Markus, C. L. Parkinson, and T. Vihma, 2012: Moisture fluxes derived from EOS aqua satellite data for the north water polynya over 2003–2009. *J. Geophys. Res.*, **117**, D06119, https://doi.org/10.1029/2011jd016949.

Campbell, E. C., E. A. Wilson, G. W. K. Moore, S. C. Riser, C. E. Brayton, M. R. Mazloff, and L. D. Talley, 2019: Antarctic offshore polynyas linked to Southern Hemisphere climate anomalies. *Nature*, **570**, 319–325, https://doi.org/10.1038/s41586-019-1294-0.

Cavalieri, D. J., and S. Martin, 1994: The contribution of Alaskan, Siberian, and Canadian coastal polynyas to the cold halocline layer of the Arctic Ocean. *J. Geophys. Res.*, **99**, 18 343–18 362, https://doi.org/10.1029/94jc01169.

——, and C. L. Parkinson, 2012: Arctic sea ice variability and trends, 1979–2010. *Cryosphere*, **6**, 881–889, https://doi.org/10.5194/tc-6-881-2012.

——, P. Gloersen, and W. J. Campbell, 1984: Determination of sea ice parameters with the NIMBUS 7 SMMR. *J. Geophys. Res.*, **89**, 5355–5369, https://doi.org/10.1029/jd089id04p05355.

——, C. L. Parkinson, P. Gloersen, J. C. Comiso, and H. J. Zwally, 1999: Deriving long-term time series of sea ice cover from satellite passive-microwave multisensor data sets. *J. Geophys. Res.*, **104**, 15 803–15 814, https://doi.org/10.1029/1999JC900081.

Comiso, J. C., D. J. Cavalieri, C. L. Parkinson, and P. Gloersen, 1997: Passive microwave algorithms for sea ice concentration: A comparison of two techniques. *Remote Sens. Environ.*, **60**, 357–384, https://doi.org/10.1016/s0034-4257(96)00220-9.

Dokken, S. T., P. Winsor, T. Markus, J. Askne, and G. Björk, 2002: ERS SAR characterization of coastal polynyas in the Arctic and comparison with SSM/I and numerical model investigations. *Remote Sens. Environ.*, **80**, 321–335, https://doi.org/10.1016/S0034-4257(01)00313-3.

Dörr, J. S., D. B. Bonan, M. Årthun, L. Svendsen, and R. C. J. Wills, 2023: Forced and internal components of observed Arctic sea-ice changes. *Cryosphere*, **17**, 4133–4153, https://doi.org/10.5194/tc-17-4133-2023.

Else, B. G. T., T. N. Papakyriakou, M. G. Asplin, D. G. Barber, R. J. Galley, L. A. Miller, and A. Mucci, 2013: Annual cycle of air-sea CO_2 exchange in an Arctic Polynya Region. *Global Biogeochem. Cycles*, **27**, 388–398, https://doi.org/10.1002/gbc.20016.

Gordon, A. L., and J. C. Comiso, 1988: Polynyas in the Southern Ocean. *Sci. Amer.*, **258**, 90–97, https://doi.org/10.1038/scientificamerican0688-90.

Gultepe, I., G. A. Isaac, A. Williams, D. Marcotte, and K. B. Strawbridge, 2003: Turbulent heat fluxes over leads and polynyas, and their effects on Arctic clouds during FIRE.ACE: Aircraft observations for April 1998. *Atmos.–Ocean*, **41**, 15–34, https://doi.org/10.3137/ao.410102.

Hersbach, H., and Coauthors, 2020: The ERA5 global reanalysis. *Quart. J. Roy. Meteor. Soc.*, **146**, 1999–2049, https://doi.org/10.1002/qj.3803.

Hirano, D., and Coauthors, 2016: A wind-driven, hybrid latent and sensible heat coastal polynya off Barrow, Alaska. *J. Geophys. Res. Oceans*, **121**, 980–997, https://doi.org/10.1002/2015JC011318.

Huntemann, M., G. Heygster, L. Kaleschke, T. Krumpen, M. Mäkynen, and M. Drusch, 2014: Empirical sea ice thickness retrieval during the freeze-up period from SMOS high incident angle observations. *Cryosphere*, **8**, 439–451, https://doi.org/10.5194/tc-8-439-2014.

Ingram, R., J. Bâcle, D. G. Barber, Y. Gratton, and H. Melling, 2002: An overview of physical processes in the North Water. *Deep-Sea Res. II*, **49**, 4893–4906, https://doi.org/10.1016/S0967-0645(02)00169-8.

Iwamoto, K., K. I. Ohshima, and T. Tamura, 2014: Improved mapping of sea ice production in the Arctic Ocean using AMSR-E thin ice thickness algorithm. *J. Geophys. Res. Oceans*, **119**, 3574–3594, https://doi.org/10.1002/2013jc009749.

Kaleschke, L., X. Tian-Kunze, N. Maaß, M. Mäkynen, and M. Drusch, 2012: Sea ice thickness retrieval from SMOS brightness temperatures during the Arctic freeze-up period. *Geophys. Res. Lett.*, **39**, L05501, https://doi.org/10.1029/2012gl050916.

Kawaguchi, Y., T. Tamura, S. Nishino, T. Kikuchi, M. Itoh, and H. Mitsudera, 2011: Numerical study of winter water formation in the Chukchi Sea: Roles and impacts of coastal polynyas. *J. Geophys. Res.*, **116**, C07025, https://doi.org/10.1029/2010jc006606.

Kohnemann, S. H. E., G. Heinemann, D. H. Bromwich, and O. Gutjahr, 2017: Extreme warming in the Kara Sea and Barents Sea during the winter period 2000–16. *J. Climate*, **30**, 8913–8927, https://doi.org/10.1175/JCLI-D-16-0693.1.

Landrum, L. L., A. K. DuVivier, M. M. Holland, K. Krumhardt, and Z. Sylvester, 2024: Defining Antarctic polynyas in satellite observations and climate model output to support ecological climate change research. *EGUsphere*, https://doi.org/10.5194/egusphere-2024-3490.

Marchese, C., C. Albouy, J.-É. Tremblay, D. Dumont, F. D'Ortenzio, S. Vissault, and S. Bélanger, 2017: Changes in phytoplankton bloom phenology over the North Water (NOW) polynya: A response to changing environmental conditions. *Polar Biol.*, **40**, 1721–1737, https://doi.org/10.1007/s00300-017-2095-2.

Martin, S., and D. J. Cavalieri, 1989: Contributions of the Siberian shelf polynyas to the Arctic Ocean intermediate and deep water. *J. Geophys. Res.*, **94**, 12 725–12 738, https://doi.org/10.1029/JC094iC09p12725.

——, R. Drucker, R. Kwok, and B. Holt, 2004: Estimation of the thin ice thickness and heat flux for the Chukchi Sea Alaskan coast polynya from Special Sensor Microwave/Imager data, 1990–2001. *J. Geophys. Res.*, **109**, C10012, https://doi.org/10.1029/2004jc002428.

Massom, R. A., P. T. Harris, K. J. Michael, and M. J. Potter, 1998: The distribution and formative processes of latent-heat polynyas in East Antarctica. *Ann. Glaciol.*, **27**, 420–426, https://doi.org/10.3189/1998AoG27-1-420-426.

Mioduszewski, J., S. Vavrus, and M. Wang, 2018: Diminishing Arctic sea ice promotes stronger surface winds. *J. Climate*, **31**, 8101–8119, https://doi.org/10.1175/JCLI-D-18-0109.1.

Mohrmann, M., C. Heuzé, and S. Swart, 2021: Southern Ocean polynyas in CMIP6 models. *Cryosphere*, **15**, 4281–4313, https://doi.org/10.5194/tc-15-4281-2021.

Monroe, E. E., P. C. Taylor, and L. N. Boisvert, 2021: Arctic cloud response to a perturbation in sea ice concentration: The North Water polynya. *J. Geophys. Res. Atmos.*, **126**, e2020JD034409, https://doi.org/10.1029/2020JD034409.

Moore, G. W. K., S. E. L. Howell, and M. Brady, 2023: Evolving relationship of Nares Strait ice arches on sea ice along the Strait and the North Water, the Arctic's most productive polynya. *Sci. Rep.*, **13**, 9809, https://doi.org/10.1038/s41598-023-36179-0.

Morales Maqueda, M. A., A. J. Willmott, and N. R. T. Biggs, 2004: Polynya dynamics: A review of observations and modeling. *Rev. Geophys.*, **42**, RG1004, https://doi.org/10.1029/2002RG000116.

Nakata, K., K. I. Ohshima, S. Nihashi, N. Kimura, and T. Tamura, 2015: Variability and ice production budget in the Ross Ice Shelf Polynya based on a simplified polynya model and satellite observations. *J. Geophys. Res. Oceans*, **120**, 6234–6252, https://doi.org/10.1002/2015jc010894.

NSIDC, 2024: Summary of SMMR, SSM/I and SSMIS sensors. NASA National Snow and Ice Data Center Distributed Active Archive Center, 6 pp., https://nsidc.org/sites/default/files/documents/technical-reference/smmr-ssmi-ssmis-sensors.pdf.

Paţilea, C., G. Heygster, M. Huntemann, and G. Spreen, 2019: Combined SMAP–SMOS thin sea ice thickness retrieval. *Cryosphere*, **13**, 675–691, https://doi.org/10.5194/tc-13-675-2019.

Pease, C. H., 1987: The size of wind-driven coastal polynyas. *J. Geophys. Res.*, **92**, 7049–7059, https://doi.org/10.1029/JC092iC07p07049.

Preußer, A., S. Willmes, G. Heinemann, and S. Paul, 2015: Thin-ice dynamics and ice production in the Storfjorden polynya for winter seasons 2002/2003–2013/2014 using MODIS thermal infrared imagery. *Cryosphere*, **9**, 1063–1073, https://doi.org/10.5194/tc-9-1063-2015.

——, G. Heinemann, S. Willmes, and S. Paul, 2016: Circumpolar polynya regions and ice production in the Arctic: Results from MODIS thermal infrared imagery from 2002/2003 to 2014/2015 with a regional focus on the Laptev Sea. *Cryosphere*, **10**, 3021–3042, https://doi.org/10.5194/tc-10-3021-2016.

——, K. I. Ohshima, K. Iwamoto, S. Willmes, and G. Heinemann, 2019: Retrieval of wintertime sea ice production in Arctic polynyas using thermal infrared and passive microwave remote sensing data. *J. Geophys. Res. Oceans*, **124**, 5503–5528, https://doi.org/10.1029/2019jc014976.

Rantanen, M., A. Y. Karpechko, A. Lipponen, K. Nordling, O. Hyvärinen, K. Ruosteenoja, T. Vihma, and A. Laaksonen, 2022: The Arctic has warmed nearly four times faster than the globe since 1979. *Commun. Earth Environ.*, **3**, 168, https://doi.org/10.1038/s43247-022-00498-3.

Ren, H., M. Shokr, X. Li, Z. Zhang, F. Hui, and X. Cheng, 2022: Estimation of sea ice production in the North Water Polynya based on ice arch duration in winter during 2006–2019. *J. Geophys. Res. Oceans*, **127**, e2022JC018764, https://doi.org/10.1029/2022jc018764.

Rinke, A., M. Maturilli, R. M. Graham, H. Matthes, D. Handorf, L. Cohen, S. R. Hudson, and J. C. Moore, 2017: Extreme cyclone events in the Arctic: Wintertime variability and trends. *Environ. Res. Lett.*, **12**, 094006, https://doi.org/10.1088/1748-9326/aa7def.

Rolph, R. J., D. L. Feltham, and D. Schröder, 2020: Changes of the Arctic marginal ice zone during the satellite era. *Cryosphere*, **14**, 1971–1984, https://doi.org/10.5194/tc-14-1971-2020.

Shen, X., C.-Q. Ke, B. Cheng, W. Xia, L. Mengmeng, X. Yu, and H. Li, 2021: Thinner sea ice contribution to the remarkable polynya formation North of Greenland in August 2018. *Adv. Atmos. Sci.*, **38**, 1474–1485, https://doi.org/10.1007/s00376-021-0136-9.

Shupe, M. D., and Coauthors, 2022: Overview of the MOSAiC expedition: Atmosphere. *Elementa*, **10**, 00060, https://doi.org/10.1525/elementa.2021.00060.

Smedsrud, L. H., W. P. Budgell, A. D. Jenkins, and B. Ådlandsvik, 2006: Fine-scale sea-ice modelling of the Storfjorden polynya, Svalbard. *Ann. Glaciol.*, **44**, 73–79, https://doi.org/10.3189/172756406781811295.

Smith, S. D., R. D. Muench, and C. H. Pease, 1990: Polynyas and leads: An overview of physical processes and environment. *J. Geophys. Res.*, **95**, 9461–9479, https://doi.org/10.1029/JC095iC06p09461.

Spreen, G., L. Kaleschke, and G. Heygster, 2008: Sea ice remote sensing using AMSR-E 89-GHZ channels. *J. Geophys. Res.*, **113**, C02S03, https://doi.org/10.1029/2005JC003384.

Tamura, T., and K. I. Ohshima, 2011: Mapping of sea ice production in the Arctic coastal polynyas. *J. Geophys. Res.*, **116**, C07030, https://doi.org/10.1029/2010JC006586.

Tian-Kunze, X., L. Kaleschke, N. Maaß, M. Mäkynen, N. Serra, M. Drusch, and T. Krumpen, 2014: SMOS-derived thin sea ice thickness: Algorithm baseline, product specifications and initial verification. *Cryosphere*, **8**, 997–1018, https://doi.org/10.5194/tc-8-997-2014.

Virtanen, P., and Coauthors, 2020: SciPy 1.0: Fundamental algorithms for scientific computing in Python. *Nat. Methods*, **17**, 261–272, https://doi.org/10.1038/s41592-019-0686-2.

Willmes, S., S. Adams, D. Schröder, and G. Heinemann, 2011: Spatio-temporal variability of polynya dynamics and ice production in the Laptev Sea between the winters of 1979/80 and 2007/08. *Polar Res.*, **30**, 5971, https://doi.org/10.3402/polar.v30i0.5971.

Zhou, L., C. Heuzé, and M. Mohrmann, 2022: Early winter triggering of the Maud Rise polynya. *Geophys. Res. Lett.*, **49**, e2021GL096246, https://doi.org/10.1029/2021GL096246.